Analytical treatment interruption after short-term anti-retroviral therapy in a postnatally SHIV infected infant rhesus macaque model.

Ria Goswami[a], Ashley N. Nelson[a], Joshua J. Tu[a], Maria Dennis[a], Liqi Feng[b], Amit Kumar[a], Jesse Mangold[a], Riley J. Mangan[a], Cameron Mattingly[c], Alan D. Curtis II[d,e], Veronica Obregon-Perko[c], Maud Mavigner[c], Justin Pollara[f], George M. Shaw[g], Katharine J. Bar[g], Ann Chahroudi[c,h], Kristina De Paris[d,e], Cliburn Chan[i], Koen K.A. Van Rompay[j], and Sallie R. Permar[a,k #].

[a]Duke Human Vaccine Institute, Duke University Medical Center, Durham, North Carolina, USA.

[b]Duke Clinical Research Institute, Duke University Medical Center, Durham, North Carolina, USA.

[c]Department of Pediatrics, Emory University School of Medicine, Atlanta, Georgia, USA

[d]Department of Microbiology and Immunology, School of Medicine, University of North Carolina at Chapel Hill, Chapel Hill, North Carolina, USA

[e]Center for AIDS Research, School of Medicine, University of North Carolina at Chapel Hill, Chapel Hill, North Carolina, USA

[f]Department of Surgery, Duke University School of Medicine, Durham, North Carolina, USA.

[g]Department of Medicine, University of Pennsylvania, Philadelphia, Pennsylvania, USA

[h]Emory+Children's Center for Childhood Infections and Vaccines, Atlanta, Georgia, USA

[i]Department of Biostatistics and Bioinformatics, Duke University Medical Center, Durham, North Carolina, USA.

[j]California National Primate Research Center, University of California, Davis, CA, USA

[k]Department of Pediatrics, Duke University School of Medicine, Durham, North Carolina, USA.

Running Title: ART interruption in SHIV-infected infant macaques.

Address correspondence to Sallie R. Permar, sallie.permar@duke.edu

R.G. and A.N.N. contributed equally to this work.

Abstract word count: 235

Text word count: 5631

ABSTRACT.

To achieve long-term viral remission in HIV-infected children, novel strategies beyond early anti-retroviral therapy (ART) will be necessary. Identifying clinical predictors of time to viral rebound upon ART interruption will streamline the development of novel therapeutic strategies and accelerate their evaluation in clinical trials. However, identification of these biomarkers is logistically challenging in infants, due to sampling limitations and potential risks of treatment interruption. To facilitate identification of biomarkers predicting viral rebound, we have developed an infant rhesus macaque (RM) model of oral SHIV.CH505.375H.dCT challenge and analytical treatment interruption (ATI) after short-term ART. We used this model to characterize SHIV replication kinetics and virus-specific immune responses during short-term ART or post-ATI and demonstrated plasma viral rebound in 5 out of 6 (83%) infants. We observed a decline in humoral immune responses and partial dampening of systemic immune activation upon initiation of ART in these infants. Furthermore, we documented that infant and adult macaques have similar SHIV replication and rebound kinetics and equally potent virus-specific humoral immune responses. Finally, we validated our models by confirming a well-established correlate of time to viral rebound, namely pre-ART plasma viral load, as well as identified additional potential humoral immune correlates. Thus, this model of infant ART and viral rebound can be used and further optimized to define biomarkers of viral rebound following long-term ART as well as to pre-clinically assess novel therapies to achieve a pediatric HIV functional cure.

69 **IMPORTANCE.**

70

71 Novel interventions that do not rely on daily adherence to ART are needed to achieve
72 sustained viral remission for perinatally infected children who currently rely on lifelong
73 ART. Considering the risks and expense associated with ART-interruption trials,
74 identification of biomarkers of viral rebound will prioritize promising therapeutic
75 intervention strategies, including anti-HIV Env protein therapeutics. However,
76 comprehensive studies to identify those biomarkers are logistically challenging in
77 human infants, demanding the need for relevant non-human primate models of HIV
78 rebound. In this study, we developed an infant RM model of oral Simian/Human
79 Immunodeficiency virus infection expressing clade C HIV Env, and short-term ART
80 followed by ATI, longitudinally characterizing immune responses to viral infection during
81 ART and post-ATI. Additionally, we compared this infant RM model to an analogous
82 adult RM rebound model and identified virologic and immunologic correlates of time to
83 viral rebound post-ATI.

84

85 Word limit: 150

86 Word count: 141

87

88

89

90

91

INTRODUCTION.

Despite the widespread availability and effectiveness of antiretroviral therapy (ART), each year >180,000 infants continue to become infected with HIV (1). Acquiring HIV at this early age commits these children to life-long ART, since stopping therapy is universally associated with viral rebound. However, continuous access to ART can be challenging in resource-limited settings (2), leading to treatment interruption and poor clinical outcomes. Maintaining adherence to life-long therapy is particularly challenging among adolescents (3), resulting in the development of drug resistant viral strains (4). Even if adherence is maintained, chronic exposure to ART from a young age predisposes children to drug-associated metabolic complications (5). Therefore, novel intervention strategies that do not rely on daily ART will be needed for sustained viral remission in infected children. While the establishment of viral reservoirs may not be prevented even when ART is initiated within hours of HIV infection (6), a reduced size of the latent reservoir has been demonstrated to lengthen time to viral rebound in clinical trials (7-9). Therefore, reducing the size of the viral reservoir and attaining sustained viral remission after treatment discontinuation has been the focus of an emerging global effort aimed at developing a cure for HIV infection.

As new therapeutic interventions to attain drug-free viral remission are developed and assessed in clinical trials, safe means to measure their efficacy will be needed. While mathematical models to predict viral rebound time from reservoir size have been developed (10-12), this approach is limited by the inaccuracy of existing assays to

115 measure viral reservoir size (13) and inter-patient variability in response to identical
116 treatment strategies. Therefore, careful monitoring of viral rebound after analytical
117 treatment interruption (ATI) still remains the “gold standard” to accurately validate the
118 efficacy of any novel HIV therapeutic strategy. However, this approach is logistically
119 challenging and carries considerable risk of virus transmission and replenishment of
120 viral reservoir upon reactivation. More importantly, this strategy will be ethically
121 challenging in HIV-infected children, since the outcome of ATI studies on long-term
122 pediatric health are not known. Considering these risks, identification of biomarkers to
123 serve as predictors of time to HIV rebound (14) would be useful to prioritize
124 development of treatment strategies, avoiding the cost and risk of ATI studies that are
125 unlikely to have clinical efficacy.
126
127 Virologic and immunologic biomarkers predicting HIV rebound have been identified by
128 several studies in recent years (15-18). Yet, our understanding of the predictors of HIV
129 rebound in the setting of maturing infant immune systems is limited. These types of
130 comprehensive studies are further complicated in infants due to limited volumes of
131 samples that can be collected at this age. Thus, pediatric rhesus macaque (RM) models
132 of HIV infection and treatment can be instrumental (19). Building on pediatric RM
133 models of breast milk transmission (20) and persistence (21) with simian
134 immunodeficiency viruses (SIVs), here we have developed a pediatric RM model of
135 ART and viral rebound using infant RMs experimentally infected with a next generation
136 chimeric simian-human immunodeficiency virus, SHIV.CH505.375H.dCT (22), that
137 would permit an assessment of interventions directed against the HIV-Env. This virus

carries a mutation in the CD4 binding site that facilitates entry via rhesus CD4 molecule that has been previously demonstrated to replicate efficiently in adult RMs (22), recapitulating the viral replication dynamics and immunopathogenesis of HIV infection in humans (23). We used the infant RM model to characterize the replication kinetics and virus-specific humoral immune responses during short-term ART and after ATI. We also utilized a unique opportunity to compare the viral and immune response kinetics of infant monkeys to that of adults infected with the same virus, during ART and post-ATI. Furthermore, we validated and assessed these RM models by examining clinically established biomarkers of time to viral rebound and explored the relationship between immune response and viral rebound. This infant RM ATI model will be a valuable addition to the HIV cure research toolbox to guide translational studies for evaluating the efficacy of therapeutic strategies towards attaining drug-free HIV remission for children.

RESULTS.

Kinetics of SHIV.CH505.375H.dCT replication in orally infected infant RMs. Six infant RMs were orally challenged with SHIV.CH505.375H.dCT (22), as described in methods. Kinetics of SHIV replication in these infants were monitored for 12 weeks post infection (w.p.i), when they were initiated on a daily subcutaneous ART regimen of tenofovir disoproxil fumerate (TDF), emtricitabine (FTC), and dolutegravir (DTG) for 8 weeks. After 8 weeks of ART, treatment was interrupted and infants were monitored for an additional 8 weeks followed by necropsy (Figure 1A).

In the acute phase of infection, plasma viral load (VL) peaked at 2 w.p.i ($6.7x10^5$-$3.2x10^7$ vRNA copies/mL of plasma), and then declined over time (Figure 1B). Most of the RMs did not achieve a stable VL set point, and 2 had plasma VL< limit of detection (LOD) of 15 copies/mL before ART initiation (Table 1). Of note, 1 of these 2 infants was most resistant to infection (Table 1), and neither had an MHC allele previously associated with SHIV control (24, 25) (Table S1). CD4+ T cell frequencies were generally stable, with a slight decrease in the median frequency between 2-3 w.p.i. (Figure S1A), similar to the transient peripheral CD4+ T cells decline in acute HIV infection.

Upon ART initiation, the infant RMs demonstrated plasma VL<LOD within 1-4 weeks and none of them had detectable plasma VLs during the short course of ART. Upon ATI, 5 of 6 infants had viral rebound within 1-6 weeks (median: 3 weeks), of which 2 demonstrated plasma VL<LOD, within 2-3 weeks of viral rebound (Table 1). Interestingly, 1 of the 2 animals with VL< 15 copies prior to ART (46367), experienced

viral rebound, post-ATI (Figure 1B). Not surprisingly, the animal with persistently high pre-ART viremia (46352) was the first to rebound post-ATI and experienced the highest rebound viremia.

SHIV.CH505.375H.dCT reservoir in peripheral lymph nodes (LNs) and PBMCs of infant RMs. We assessed the size of viral reservoirs of infant RMs while they were virologically controlled on ART. SHIV DNA was quantified in peripheral LN-associated naïve, memory, and T follicular helper (Tfh) CD4+ T cells after 8 weeks of ART. Viral DNA was detected in all three CD4+ T cell populations in a subset of animals, with 4 of 6 monkeys having detectable DNA in naïve CD4+ T cells, 3 of 6 monkeys in memory CD4+ T cells, and 2 of 6 monkeys in Tfh cells (Figure 1C). Finally, we measured cell-associated SHIV-DNA (CA-SHIV DNA) and cell-associated SHIV-RNA (CA-SHIV RNA), per million CD4+ T cells isolated from PBMCs using digital droplet PCR (ddPCR). Of note, we could only report CA-SHIV DNA and CA-SHIV RNA data for those animals which had input cell counts greater than the threshold cell count for the assay (see methods). Our data demonstrated a decrease in CA-SHIV DNA (Figure 1D) and -SHIV RNA/million CD4+ T cells (Figure 1E), with only one infant (46352) having detectable CA-SHIV RNA, after 6 weeks of ART.

Anatomic distribution of SHIV.CH505.375H.dCT post rebound in infant RMs. As anatomic sites of viral replication after ATI might reveal major sources of viral rebound, we sought to determine the distribution of SHIV.CH505.375H.dCT in blood and tissue compartments, at necropsy. Cell-associated infectious SHIV was measured in oral and

gut-associated tissues (8 weeks post-ATI) using a Tzm-bl based co-culture assay (Figure S2), and 50% cellular infectious dose (CID_{50}) for each tissue was reported (see methods). Our data demonstrated that the infectious virus was primarily distributed in the LNs and gut-associated tissues, compared to spleen (Figure 2A), which might be attributed to the lower proportion of CD4+ T cells in spleen (Figure S1B), vs. LNs. Interestingly, a higher number of animals had infectious virus detectable in oral LN (submandibular LN) compared to mesenteric LN and no cell-associated infectious virus was detected in PBMCs.

Eight weeks post-ATI, tissue-associated SHIV DNA and -RNA per million CD4+ T cells were detectable at variable levels (SHIV DNA: 1-3x10^4 copies/million CD4+ T cells and SHIV RNA: 1-8.61x10^3 copies/million CD4+ T cells) (Figure 2B and 2C). None of the monkeys had detectable SHIV RNA in PBMCs, further confirming our co-culture-based tissue-associated infectious viral load data. We further defined the anatomic distribution of CD3+SHIV+ cells in LN and gut-associated lymphoid tissues (GALT) of the infant that showed the highest plasma VL, post rebound, using a dual immunohistochemistry (IHC)/ in situ hybridization (ISH) approach (Figure 2D). Interestingly, CD3+SHIV+ cells were detected within the B cell follicles in addition to the T cell zone, suggesting that resident Tfh cells in both the tonsil and GALT can support viral replication.

Adult RMs have comparable SHIV.CH505.375H.dCT replication kinetics, viral reservoir, and rebound-virus distribution compared to infants. We took the opportunity to compare the viral replication kinetics and reservoir in infant RMs to that of

adult RMs infected with the same SHIV strain from a separate study, and thus a cohort of convenience (26). Six adult RMs, were intravenously infected with SHIV.CH505.375H.dCT (see methods) and started on triple ART regimen of TDF, FTC and DTG at 12 w.p.i. After 12 weeks of ART, therapy was discontinued, and the animals were euthanized 8 weeks post-ATI (Figure 3A). Similar to infant RMs, plasma VL in adults peaked at 2 w.p.i ($3x10^5$-$1.2x10^7$ copies of vRNA/mL of plasma). Additionally, the overall kinetics of plasma VL during acute SHIV infection was highly comparable between the two groups (Figure 3B). Upon ART initiation, plasma VL in adults was below LOD (<15 copies/mL plasma) within 1-4 weeks, with one monkey experiencing a viral blip (>15 copies/mL plasma), during the course of ART. Even though the ART regimen in adults was slightly longer than infants, 3 of 6 adults showed viral rebound within 2-3 weeks post-ATI. Interestingly, 1 of 3 adults that experienced viral rebound demonstrated plasma VL below LOD at 8 weeks post-ATI (Table 1).

SHIV reservoir was detectable in adults in naïve, memory, and Tfh CD4+ T cell subsets of peripheral LNs. (Figure 3C). As observed with infant RMs, CA-SHIV DNA (Figure 3D) and CA-SHIV RNA/million CD4+ T cells (Figure 3E) declined upon ART, with only 2 adults demonstrating detectable CA-SHIV DNA levels after 6 weeks on ART. Like infant RMs, co-culture assays detected higher infectious viral titers in oral LN (submandibular) compared to mesenteric LN, whereas cell-associated infectious virus was not detected in PBMCs (Figure 4A). CA-SHIV DNA and RNA were detected in tissues at variable levels, with none of the animals having detectable CA-SHIV RNA in PBMCs (Figure 4B and 4C). Similar to infants, the tonsils and colon lymphoid aggregates of the adult RM that showed highest plasma VL post-rebound had

detectable CD3+SHIV+ cells within the B cell follicle, in addition to T cell zone at necropsy (Figure 4D).

Viral diversity before ART initiation and post-ATI in infant and adult RMs. As the viral kinetics during acute infection, ART, and post-ATI were similar in infant and adult monkeys, we next sought to compare plasma viral Env diversity between the infant (46352) and adult RM (39950) that showed highest plasma VL post-rebound. We performed single genome amplification (SGA) and sequencing of the *env* gene pre-ART and post-ATI from plasma and calculated average pairwise distance (APD) within Env sequences. In the infant 46352, pre-ART (12 w.p.i) viral Env was more homogeneous (average pairwise distance: APD: 0.0006), compared to 2 weeks (APD: 0.0018) or 8 weeks post-ATI viral Env (APD:0.0038) (Figure 5A). In contrast, for the adult 39950, pre-ART viral Env (12 w.p.i) had a 4-fold higher diversity (APD: 0.004), compared to 2 weeks post-ATI viral Env (APD: 0.001) (Figure 5B).

ART dampens the magnitude of humoral responses in SHIV-infected infant and adult RMs. As previous reports have noted a loss of HIV-specific humoral responses in human infants on ART (27), we investigated differences in the kinetics, magnitude, and breadth of the Env-specific humoral responses on ART and following ATI between the age groups. In both age groups, all monkeys developed detectable autologous gp120-specfic IgG responses at 12 w.p.i. (Figure 6A). After 8 weeks of ART, gp120-specific IgG response declined in both groups, the decline being more pronounced in infants. Yet, the gp120-specific IgG response rebounded in both groups post-ATI. Interestingly,

the infant (46359) with plasma VL<15 copies pre-ART and no viral rebound, developed similar gp120-specific IgG response to that of other infants. We then mapped the Env-domain specificity of the antibody responses, and observed dominant responses against the V3 and -C5 linear epitopes in both groups (Figure S3), which was not altered upon ART. Interestingly, ART initiation completely abrogated plasma antibodies against the CD4 binding site and only 2 of 6 infants and no adults regained this response within the 8 weeks of follow-up after ART was discontinued. (Figure 6B).

We next evaluated the HIV neutralization potency of RM plasma against a tier-1 clade-matched isolate MW965 and the autologous tier-2 CH505 virus. Both infants and adults developed neutralization activity against MW965 by 12 w.p.i, which continued to increase post- ATI, with equal potency between age groups (Figure 6C). However, only half of both the adult and infant RMs had a detectable neutralization response against autologous CH505 at 12 w.p.i. (Figure 6D). Post-ATI, 2 of 6 infants and 4 of 6 adults demonstrated increasing neutralization responses against the autologous virus. In both age groups, gp120- specific ADCC titers dampened upon ART initiation, yet recovered to pre-ART levels after ATI (Figure 6E).

T cell activation during ART in infant and adult RMs. Systemic immune activation has been associated with HIV replication and poor disease outcomes (28). Furthermore, T cell exhaustion markers have been reported as predictors of viral rebound in a human study (15). Therefore, we assessed the activation and exhaustion status of T cells from SHIV-infected, infant and adult RMs. Unlike adults, infant-activated, -proliferating and -exhausted CD4+ T cell populations increased at 10 w.p.i compared to pre-infection

299 levels, which might be attributed to the age-specific development of T cell populations
300 (Figure 7A and 7B).

301 Furthermore, we measured the concentrations of inflammatory chemokines and
302 cytokines in RM plasma pre-ART (12 w.p.i) and on ART (8 weeks of ART). While infant
303 plasma demonstrated a higher magnitude and breadth of cytokine and chemokine
304 levels than adults, no notable difference was observed pre-ART vs. on ART in both age
305 groups (Figure 7C).

306

307 **Correlates of time to SHIV rebound in infant and adult RMs.** To validate our
308 established RM SHIV rebound models in identifying correlates of time to viral rebound,
309 we performed a univariate cox-proportional hazard modeling on a subset of the
310 measured virologic and immunologic parameters, after adjustment for age. We defined
311 time to viral rebound as a plasma VL >10 times LOD (150 copies/mL) post-ART
312 discontinuation. Plasma VL pre-ART, ADCC antibodies, CD4+ CD69+ T cells and
313 autologous virus neutralizing antibodies were pre-selected as primary parameters
314 based on their previously published associations with rate of HIV acquisition (29, 30)
315 and disease progression (31, 32). Of these parameters, higher levels of plasma VL pre-
316 ART and ADCC antibody titers on ART demonstrated associations with increased risk
317 of viral rebound (Table 2). Next, we applied the model on an additional set of virologic
318 and immunologic parameters. The analysis identified higher levels of CH505 gp120-
319 specific IgG responses pre-ART and on ART, tier-1 MW965 neutralizing antibody titer,
320 and %sCD4 blocking antibodies pre-ART to be associated with higher risk of rebound

(Table 2), suggesting that our macaque models were suitable for monitoring correlates of viral rebound.

Finally, we wanted to determine the differential impact of age on the correlates of viral rebound. Due to the relatively small sample size of the two age groups, we performed Kendall's Tau rank correlation of each of the experimental parameters with viral rebound. In infants, lower plasma VL at ART start was associated with longer time to viral rebound and a correlation trend for longer time to viral rebound was observed for infant RMs with lower CH505 gp120-specific IgG responses pre-ART and on ART. In adults, lower values of plasma VL at ART start, peak plasma VL, CH505 gp120-specific IgG response pre-ART and Tier-1 MW965 neutralizing antibody titer at ART start were associated with longer time to rebound. Additionally, a correlation trend for longer time to viral rebound was observed for adult monkeys with lower CH505 gp120-specific IgG responses on ART (Table 3).

DISCUSSION.

Identification of plasma viral RNA (31) and CD4+ T cell counts (33) as surrogate markers of HIV disease progression were instrumental in the development of ART for attaining improved clinical care in HIV-infected patients. As the HIV field rapidly turns towards achieving functional “cure”, there has been renewed interest in identifying biomarkers of viral rebound. Monitoring biomarkers will guide clinical trials with effective therapeutic candidates, minimizing investment to those that are unlikely to result in delay of viral rebound. However, ATI trials for identification of biomarkers remain logistically challenging, particularly in children, necessitating the development of tractable pediatric animal models. While pediatric ATI models of SIV-infected RMs are not new to the HIV field (34), clinically translatable RM models of ATI using SHIVs have been advancing (35). Thus, we have sought to establish an oral SHIV-infected infant ATI model with a previously validated ART regimen (21).

This study investigated the impact of ART on SHIV replication and SHIV-specific immune responses in the context of the maturing infant immune system. Employing an adult RM SHIV-infected cohort of convenience, we also demonstrated that infant and adult RMs have a comparable SHIV replication kinetics and are equally equipped in mounting immune responses, both on ART and post-ATI. Furthermore, we validated our RM ATI models by confirming previously reported virologic correlates of rebound and identified additional potential humoral immune correlates.

In this study, the infant and adult RMs were infected with a clade C SHIV variant, SHIV.CH505.375H.dCT, due to the predominance of clade C viruses in sub-Saharan Africa, where most pediatric HIV infections occur (36). In both infant and adult models, this SHIV variant achieved a peak viral load comparable to previously described SIV/SHIV models (21, 37), yet did not achieve a viral "set point" in most of the monkeys (Figure 1B and 3B). Additionally, a few monkeys from our cohort achieved natural virologic control, which is not uncommon in previously described SHIV infection models (38, 39). Moreover, our study revealed a comparable plasma VL and rebound kinetics in the two age groups.

Previous studies have claimed that infants may have impaired immune responses to HIV infection compared to adults (40). However, we previously demonstrated that vaccination of infants can induce robust HIV Env-specific IgG responses (41). Moreover, we recently reported that infant monkeys are capable of mounting durable anti-HIV humoral immune responses during acute SHIV infection, despite their maturing immune landscape (26). In this study, we observed comparable humoral immune responses between the two age groups during ART and post-ATI (Figure 6). Interestingly, a decline of HIV gp120-specific IgG responses and ADCC responses were observed on ART, without a change in the specificities of the Env domain-specific antibodies (Figure S3). A similar observation was made in human infants, where HIV-specific antibody levels decreased as the duration of ART increased (42), suggesting that circulating HIV antigen is a major driving factor for production of HIV Env-specific antibodies. In fact, plasma Env-specific IgG levels could provide a more comprehensive

390 measure of viral replication in tissue sanctuaries which might not be reflected in the
391 plasma viral load.
392
393 To identify correlates of viral rebound in infants and adults, we analyzed a
394 comprehensive panel of 25 virologic and immunologic parameters. Our data confirmed
395 a key, well-established clinical virologic marker, pre-ART plasma VL, as a correlate of
396 viral rebound in both the age groups. Additionally, higher peak plasma VL was identified
397 as a correlate of quicker viral rebound in adults, but not infants. This association of pre-
398 therapy plasma VL with viral rebound has been demonstrated previously in an HIV gag-
399 based therapeutic trial, where lower pre-ART plasma VL was independently associated
400 with a lower post-ATI plasma VL (43). Among the immunologic parameters tested, in
401 adults, higher gp120-specific IgG responses and neutralizing antibodies against a tier-1
402 virus correlated with quicker viral rebound, whereas in infants higher gp120-specific IgG
403 responses, but not neutralizing antibodies against a tier-1 virus showed a correlation
404 trend with quicker viral rebound. There has been continued interest in considering anti-
405 HIV gp120 responses as a screening marker for ongoing viral replication or
406 breakthrough, during suppressive ART (44). Additionally, heterologous neutralizing
407 antibody responses at the time of treatment interruption has been associated with
408 reduced viral load over time (45). However, these identified humoral responses have
409 not been previously associated with time to viral rebound, and therefore, should be
410 examined in future long-term studies. In resource limited settings, monitoring HIV-
411 specific humoral responses in infants on suppressive ART might be beneficial due to

412 small sample volume requirement and relatively low cost and technology burden
413 compared to nucleic acid-based assays or quantitative viral outgrowth assays (QVOA).
414
415 There were a few notable limitations of this pilot study. Firstly, the adult RM model of
416 SHIV rebound used in the study was not originally designed for a direct comparison with
417 the infant ATI model (e.g., infection route, infection dose and weeks of therapy were not
418 precisely matched to the infant study). Yet, the availability of a comparable adult cohort
419 infected with the same SHIV variant and similar viral replication kinetics provided us a
420 unique opportunity to investigate the differences in infant immune responses during and
421 after therapy with respect to adults. We also acknowledge that differences in the
422 challenge route and duration of ART in adult RMs might have limited our ability to
423 directly compare the immune responses in the two age groups. Moreover, relatively
424 small cohort sizes likely contributed to our inability to identify some of the previously
425 established immunologic parameters of viral rebound such as pre-therapy levels of T
426 cell exhaustion markers: Tim-3, Lag-3 and PD-1 (15). Hence, further validation of this
427 model in larger pediatric RM cohorts will be required. Secondly, since our cohorts were
428 subjected to very short duration of ART (8-12 weeks), the measured viral reservoir
429 might not be a reflection of the true persistent reservoir on long-term suppressive ART.
430 Therefore, we have excluded measures of viral reservoir size, which have been
431 identified as predictors of viral rebound in previous adult clinical trials (16-18, 46).
432 Finally, low cell numbers collected, and the comprehensive nature of the study has
433 restricted our ability to measure longitudinal T cell functions, potentially missing T cell
434 function-associated correlates of viral rebound time.

In conclusion, this study validated an oral SHIV-infected pediatric infant RM model of ATI and characterized SHIV replication and humoral immune responses during and post-ATI. Larger and longer-term prospective studies will be needed to further optimize this model and identify a comprehensive set of biomarkers that can reliably predict time to viral rebound. Developing algorithms by combining several surrogate markers of viral rebound could greatly accelerate the process of screening children as candidates for ATI trials, and for development of novel therapeutics for HIV cure research. Additionally, an infant HIV rebound model will be a valuable tool to identify and evaluate the potency of novel therapeutic strategies for attaining functional cure in the context of the maturing infant immune system.

458 **MATERIALS AND METHODS.**

459

460 **Animal care and study design.** Type D retrovirus-, SIV- and STLV-1 free Indian
461 rhesus macaques (RM) (*Macaca mulatta*) were maintained in the colony of California
462 National Primate Research Center (CNPRC, Davis, CA), as previously described (47).
463 Six infant RMs were orally challenged with SHIV.CH505.375H.dCT (22) as described in
464 (26). Briefly, the infant RMs were challenged at 4 weeks of age by bottle feeding 3
465 times/day for 5 days at a dose of $8.5X10^4$ $TCID_{50}$, to mimic breast milk transmission.
466 After one week of challenges, 1 infant became infected. The remaining 5 were sedated
467 and orally challenged weekly at a dose of $6.8x10^5$ $TCID_{50}$. Within three weeks, 4 more
468 became infected and the final one was challenged at increasing doses ($1.3x10^6$ $TCID_{50}$,
469 followed by $3.4x10^6$ $TCID_{50}$) until infected at 14 weeks of age (Table 1). Six adult RMs
470 (age between 4-10 years), were intravenously infected with SHIV.CH505.375H.dCT at a
471 dose of $3.4x10^5$ $TCID_{50}$ as described in (26). The plasma viral RNA load of the monkeys
472 were assessed by highly sensitive qRT-PCR (48). A co-formulation containing 5.1
473 mg/kg tenofovir disoproxil fumarate (TDF), 40 mg/kg emtricitabine (FTC) and 2.5 mg/kg
474 dolutegravir (DTG) was prepared as described previously (49) and administered once
475 daily by the subcutaneous route starting 8 weeks (infants) or 12 weeks (adults), post-
476 infection (w.p.i).

477

478 **Collection and processing of blood and tissue specimens and MHC typing of**
479 **animals**. Animals were sedated with ketamine HCl (Parke-Davis) injected at 10 mg/kg
480 body weight. EDTA-anticoagulated blood was collected via peripheral venipuncture.

Plasma was separated from whole blood by centrifugation. Tissues were either fixed in formalin for *in situ* hybridization, or mononuclear cells were isolated from the tissues by density gradient centrifugation as described in (37). DNA extracted from splenocytes was used to screen for the presence of the major histocompatibility complex (MHC) class I alleles Mamu-A*01 and -B*01 and -B*08, using a PCR-based technique (50, 51).

CD4+ T cell subpopulation sorting and cell-associated SHIV DNA and RNA quantification. $CD4^+$ T cells were enriched from PBMCs and tissue mononuclear cells using a negative selection magnetic-activated cell sorting (MACS) system as per manufacturer's instructions (Miltenyi Biotec, Germany). Enriched $CD4^+$ T-cells were stained with fluorescently conjugated antibodies listed in Table S2, and sorted for naïve, memory and Tfh CD4+ T cell subsets (Figure S4). Total RNA and genomic DNA were isolated using the RNeasy Mini Kit and DNeasy Blood and Tissue Kit, respectively (Qiagen, Germany). Viral cDNA was generated from the extracted total RNA using SuperScript III reverse transcriptase enzyme (Invitrogen, Carlsbad, CA), PCR nucleotides (NEB, MA) and Gag-specific reverse primer (Table S3). SHIV-DNA and RNA/million CD4+ T cells in blood and necropsy tissues were estimated by amplifying cDNA and genomic DNA with primers and probes described in Table S3, using digital droplet PCR (ddPCR) as described in (37). The sensitivity of the ddPCR assay was estimated to be detection of 1 SHIV gag copy in 10,000 uninfected CD4+ T cells. Therefore, an input CD4+ T cell count of 10,000 was defined as threshold cell count (TCC) for the analysis, and samples having input cells< TCC were not analyzed. SHIV DNA/million CD4+ T cells was estimated after normalizing SHIV gag copy numbers with

504 input CD4+ counts. Quantification of SHIV DNA in peripheral lymph node-associated
505 naïve, memory and Tfh CD4+ T cell population was performed by qPCR as described in
506 (21), using primers and probes described in Table S3.
507
508 **Measurement of HIV Env- specific antibody responses by Enzyme-Linked**
509 **Immunosorbent Assay (ELISA).** The plasma concentrations of HIV Env-specific
510 antibodies were estimated by ELISA, as previously described (29). Human CH22
511 monoclonal antibody was used as standard and the concentration of HIV Env-specific
512 IgG antibody was calculated relative to the standard using a 5-parameter fit curve
513 (SoftMax Pro 7). The positivity cut off for the assay was defined as the optical density
514 (OD) of the lowest-concentration rhesus IgG standard that was greater than three times
515 the average OD of blank wells. CD4 blocking ELISAs were done as described in (47).
516
517 **HIV-1 Env-specific IgG epitope specificity and breadth using binding antibody**
518 **multiplex assay (BAMA).** HIV antigens were covalently conjugated to polystyrene
519 beads (Bio-Rad), and binding of IgG to the bead-conjugated HIV-1 antigens was
520 measured in RM plasma samples (29). The antigens used for the assay have been
521 described in (26). Purified IgG from pooled plasma of HIV-1 vaccinated macaques
522 (RIVIG) was used as positive control.
523
524 **Neutralization assays.** Neutralization of MW965.LucR.T2A.ecto/293T IMC (clade C,
525 tier 1) and the autologous CH505.TF (clade C, tier 2) HIV-1 pseudovirus by plasma
526 antibodies was measured in TZM-bl cells as previously described (29, 52, 53). The ID_{50}

was calculated as described in (26). The monoclonal antibody, b12R1, was used as a positive control for MW965 virus, and VRC01 was used a positive control for CH505 T/F virus.

ADCC-GranToxiLux (GTL) Assay. The ADCC-GTL assay was used to measure plasma ADCC activity as previously described (47, 54). CEM.NKR$_{CCR5}$ target cells were coated with recombinant CH505 gp120. Adult and infant plasma samples were tested after a 4-fold serial dilution starting at 1:100.

Single Genome Amplification (SGA) SGA of plasma virus was done as previously described (55). Primer used for cDNA preparation was SHIVEnv.R3out. A first round of PCR amplification was conducted using primers SIVmac.F4out and SHIVEnv.R3out A second round of PCR was conducted using primers SIVmac766.F2in and SIVmac766.R2in (Table S3). *Env* gene amplicons obtained were sequenced by Sanger sequencing, and phylogenetic tree were constructed for the aligned *env* gene sequences by neighbor-joining method using Seaview (56). Average pairwise distance was calculated using the MEGA6 software (57).

Tissue-associated infectious viral titers by co-culture assay. Serial dilutions of RM lymphoid and gut-associated mononuclear cells were co-cultured with Tzm-bl reporter cells as described previously (37) (Figure S2). Fifty percent cellular infectious dose (CID_{50}) was calculated as the number of mononuclear cells per 10^4 mononuclear cells required to yield detectable infection of 50% Tzm-bl cells, using Reed-Muench method.

The detection threshold of the assay was established as 2.5 times the mean luminescence output of Tzm-bl only cells from 10 independent experiments (876 RLU).

***In situ* hybridization (ISH).** Formalin fixed, paraffin embedded tissue sections were seqentially cut (5 µm) and stained for CD3 and CD20 (Table S2) as previously described (58, 59). SHIV RNA was visualized with the 1-Plex ViewRNA^{TM} ISH Tissue Assay Kit using SIV_{mac239} or Beta actin (positive control) probe sets and ViewRNA Chromogenic Signal Amplification Kit (ThermoFisher, Waltham, MA). These two sequential slides were indivudually imaged with a Zeiss AxioObserver microscope and AxioCam MRm camera. Composite overlays of CD3/CD20 stained slides with ISH slides were prepared using Zen Lite v2.3 software (Zeiss).

T cell phenotyping. Phenotyping of rhesus PBMCs and tissue-associated mononuclear cells were performed as described previously (37). Fluorescently-conjugated antibodies used to stain cells are reported in Table S2. For intercellular staining, cells were fixed and permeabilized using eBioscience^{TM} FoxP3/transcription factor staining buffer set (Thermo Fisher Scientific), according to manufacturer's instructions. The stained cells were acquired on an LSRII flow cytometer (BD Biosciences) using BD FACS Diva software and analyzed with FlowJo software version 10 (Tree Star, Inc). Gating for all surface and intracellular markers (Figure S4) was based on fluorescence minus one (FMO) controls. Complete blood counts (CBC) were performed on EDTA-anticoagulated blood samples. Samples were analyzed using a Pentra 60C+ analyzer (ABX Diagnostics). Absolute lymphocyte counts in blood were

573 calculated using the PBMC counts obtained by automated complete blood counts,
574 multiplied by the lymphocyte percentages.
575
576 **Multiplex analysis of plasma cytokines and chemokines.** Plasma cytokine and
577 chemokine concentrations were assayed in duplicate using a MIP-1α singleplex kit and
578 a 22-analyte multiplex panel (G-CSF, GM-CSF, IFN-γ, IL-1RA, IL-1β, IL-2, IL-4, IL-5, IL-
579 6, IL-8, IL-10, IL-12/23 (p40), IL-13, IL-15, IL-17, IL-18, MCP-1, MIP-1β, sCD40L, TGF-
580 α, TNF-α, VEGF) (both Millipore PRCYTOMAG-40K) performed according to the
581 manufacturer's recommended protocol and read using a FlexMAP 3D array reader
582 (Luminex Corp.). Data were analyzed using Bio-Plex Manager software (Bio-Rad).
583
584 **Statistical analysis.** Differences in immune assay measurements between pre-
585 identified time points post-infection were performed by Wilcoxon signed-rank test using
586 the R language and environment for statistical computing (60). Four responses were
587 pre-selected as primary variables of interest. Additionally, 5 virologic and humoral
588 response-associated variables and 16 T cell phenotype and plasma inflammatory
589 response-associated variables were selected for exploratory analysis. Cox proportional
590 hazards modeling was used to create univariate survival models for each variable,
591 treating time to rebound as the event of interest. To account for differences between
592 adult and neonate groups, a binary indicator for the two different groups was used as a
593 control variable. To identify correlates of viral rebound in infants and adults, Kendall's
594 tau between every variable of interest and the time to virus rebound was computed.

595 Raw p-values and/or FDR-adjusted (Benjamini-Hochberg) p-values, and hazard ratios
596 with confidence intervals were reported for each variable.
597
598 **ACKNOWLEDGEMENTS.**
599
600 The work was supported by National Institutes of Health grants P01 AI117915 (S.R.P.
601 and K.D.P.); 5R01 AI106380 (S.R.P.); T32 5108303 (A.D.C.) and 5R01-DE025444
602 (S.R.P.). This work was also supported by the Penn Center for AIDS Research Viral
603 and Molecular Core P30 AI045008 (K.J.B.); the BEAT-HIV: Delaney Collaboratory to
604 Cure HIV-1 Infection by Combination Immunotherapy UM1AI126620 (K.J.B.); and
605 CARE: Delaney Collaboratory for AIDS Eradication UM1AI126619 (K.J.B.) and the
606 Office of Research Infrastructure Program/OD (P51OD11107; CNPRC). The research
607 contributions by A.D.C. and K.D.P. were supported by the University of North Carolina
608 at Chapel Hill Center for AIDS Research (CFAR), and NIH funded program P30
609 AI050410. The funders had no role in study design, data collection and interpretation, or
610 the decision to submit the work for publication. The content is solely the responsibility of
611 the authors and does not necessarily represent the official views of the National
612 Institutes of Health.

613 Several protein antigens for BAMAs and ELISAs were generously provided by
614 Dr. Barton Haynes, supported by NIH NIAID Division of AIDS UM1 grant AI100645 for
615 the Center for HIV/AIDS Vaccine Immunology-Immunogen Discovery (CHAVI-ID), and
616 produced at the Duke Human Vaccine institute (DHVI) Protein Production Facility. We
617 thank Dr. Jeff Lifson, Rebecca Shoemaker and colleagues in the Quantitative Molecular

Diagnostics Core of the AIDS and Cancer Virus Program of the Frederick National Laboratory for expert assistance with viral load measurements. We would like to thank Jennifer Watanabe, Dr. Amir Ardeshir and the staff of the CNPRC Colony Research Services for their support in these studies. We thank Emory University Pediatrics/Winship Flow Cytometry Core for technical assistance with CD4+ T cell subpopulation sorting and Center for AIDS Research at Emory University (P30AI050409) for qPCR assays. We thank Papa Kwadwo Morgan-Asiedu, Joshua A. Eudailey, Holly Heimsath and Shuk Hang (Grace) Li at DHVI for assisting with animal tissue processing. We would also like to thank DHVI Regional Biocontainment laboratory (RBL) for technical support with multiplex assay for measuring plasma cytokine response, and R. Whitney Edwards and Nicole Rodgers for performing ADCC assays. T cell phenotyping was performed in the DHVI Flow Cytometry Facility (Durham, NC).

AUTHOR DISCLOSURE STATEMENT. No competing financial interests.

AUTHOR CONTRIBUTIONS. R.G., A.N.N., K.D.P., K.K.A.V.R. and S.R.P. designed the study and interpreted the data; R.G., A.N.N., J.J.T., M.D., A.K., J.M., R.J.M., C.M., A.D.C., V.O.P., M.V. and J.P. performed the experiments and analyzed the data; L.F. and C.C. performed the statistical analysis; G.M.S. and K.J.B. provided virus and consulted on the infection model; A.C., K.D.P. and K.K.A.V.R. contributed important insights for the interpretation and discussion of the results. R.G. and S.R.P. drafted the manuscript. All authors read and approved the final manuscript.

641

642 **REFERENCES.**

643

644 1. UNAIDS. Global HIV & AIDS statistics — 2018 fact sheet 2018. Available from:
645 http://www.unaids.org/en/resources/fact-sheet.
646 2. UNAIDS. Access to antiretroviral therapy in Africa-Status report on progress
647 towards the 2015 targets. Available from:
648 http://www.unaids.org/sites/default/files/media_asset/20131219_AccessARTAfricaStatu
649 sReportProgresstowards2015Targets_en_0.pdf.
650 3. Kim SH, Gerver SM, Fidler S, Ward H. Adherence to antiretroviral therapy in
651 adolescents living with HIV: systematic review and meta-analysis. AIDS.
652 2014;28(13):1945-56. Epub 2014/05/23. doi: 10.1097/QAD.0000000000000316.
653 PubMed PMID: 24845154; PubMed Central PMCID: PMCPMC4162330.
654 4. Viani RM, Peralta L, Aldrovandi G, Kapogiannis BG, Mitchell R, Spector SA, Lie
655 YS, Weidler JM, Bates MP, Liu N, Wilson CM, Adolescent Medicine Trials Network for
656 HIVAI. Prevalence of primary HIV-1 drug resistance among recently infected
657 adolescents: a multicenter adolescent medicine trials network for HIV/AIDS
658 interventions study. The Journal of infectious diseases. 2006;194(11):1505-9. Epub
659 2006/11/04. doi: 10.1086/508749. PubMed PMID: 17083034.
660 5. Barlow-Mosha L, Eckard AR, McComsey GA, Musoke PM. Metabolic
661 complications and treatment of perinatally HIV-infected children and adolescents. J Int
662 AIDS Soc. 2013;16:18600. Epub 2013/06/21. doi: 10.7448/IAS.16.1.18600. PubMed
663 PMID: 23782481; PubMed Central PMCID: PMCPMC3691550.

664 6. Luzuriaga K, Gay H, Ziemniak C, Sanborn KB, Somasundaran M, Rainwater-
665 Lovett K, Mellors JW, Rosenbloom D, Persaud D. Viremic relapse after HIV-1 remission
666 in a perinatally infected child. The New England journal of medicine. 2015;372(8):786-8.
667 doi: 10.1056/NEJMc1413931. PubMed PMID: 25693029; PubMed Central PMCID:
668 PMC4440331.
669 7. Yukl SA, Boritz E, Busch M, Bentsen C, Chun TW, Douek D, Eisele E, Haase A,
670 Ho YC, Hutter G, Justement JS, Keating S, Lee TH, Li P, Murray D, Palmer S, Pilcher
671 C, Pillai S, Price RW, Rothenberger M, Schacker T, Siliciano J, Siliciano R, Sinclair E,
672 Strain M, Wong J, Richman D, Deeks SG. Challenges in detecting HIV persistence
673 during potentially curative interventions: a study of the Berlin patient. PLoS pathogens.
674 2013;9(5):e1003347. doi: 10.1371/journal.ppat.1003347. PubMed PMID: 23671416;
675 PubMed Central PMCID: PMC3649997.
676 8. Henrich TJ, Hanhauser E, Marty FM, Sirignano MN, Keating S, Lee TH, Robles
677 YP, Davis BT, Li JZ, Heisey A, Hill AL, Busch MP, Armand P, Soiffer RJ, Altfeld M,
678 Kuritzkes DR. Antiretroviral-free HIV-1 remission and viral rebound after allogeneic stem
679 cell transplantation: report of 2 cases. Annals of internal medicine. 2014;161(5):319-27.
680 doi: 10.7326/M14-1027. PubMed PMID: 25047577; PubMed Central PMCID:
681 PMC4236912.
682 9. Persaud D, Gay H, Ziemniak C, Chen YH, Piatak M, Jr., Chun TW, Strain M,
683 Richman D, Luzuriaga K. Absence of detectable HIV-1 viremia after treatment cessation
684 in an infant. The New England journal of medicine. 2013;369(19):1828-35. doi:
685 10.1056/NEJMoa1302976. PubMed PMID: 24152233; PubMed Central PMCID:
686 PMC3954754.

687 10. Hill AL, Rosenbloom DI, Fu F, Nowak MA, Siliciano RF. Predicting the outcomes
688 of treatment to eradicate the latent reservoir for HIV-1. Proceedings of the National
689 Academy of Sciences of the United States of America. 2014;111(37):13475-80. Epub
690 2014/08/07. doi: 10.1073/pnas.1406663111. PubMed PMID: 25097264; PubMed
691 Central PMCID: PMCPMC4169952.
692 11. Hill AL, Rosenbloom DI, Goldstein E, Hanhauser E, Kuritzkes DR, Siliciano RF,
693 Henrich TJ. Real-Time Predictions of Reservoir Size and Rebound Time during
694 Antiretroviral Therapy Interruption Trials for HIV. PLoS pathogens.
695 2016;12(4):e1005535. Epub 2016/04/28. doi: 10.1371/journal.ppat.1005535. PubMed
696 PMID: 27119536; PubMed Central PMCID: PMCPMC4847932.
697 12. Pinkevych M, Kent SJ, Tolstrup M, Lewin SR, Cooper DA, Sogaard OS,
698 Rasmussen TA, Kelleher AD, Cromer D, Davenport MP. Modeling of Experimental Data
699 Supports HIV Reactivation from Latency after Treatment Interruption on Average Once
700 Every 5-8 Days. PLoS pathogens. 2016;12(8):e1005740. doi:
701 10.1371/journal.ppat.1005740. PubMed PMID: 27560972; PubMed Central PMCID:
702 PMC4999223.
703 13. Siliciano JD, Siliciano RF. Assays to Measure Latency, Reservoirs, and
704 Reactivation. Current topics in microbiology and immunology. 2018;417:23-41. doi:
705 10.1007/82_2017_75. PubMed PMID: 29071475.
706 14. Li JZ, Smith DM, Mellors JW. The need for treatment interruption studies and
707 biomarker identification in the search for an HIV cure. AIDS. 2015;29(12):1429-32. Epub
708 2015/04/15. doi: 10.1097/QAD.0000000000000658. PubMed PMID: 25870989;
709 PubMed Central PMCID: PMCPMC4529360.

15. Hurst J, Hoffmann M, Pace M, Williams JP, Thornhill J, Hamlyn E, Meyerowitz J, Willberg C, Koelsch KK, Robinson N, Brown H, Fisher M, Kinloch S, Cooper DA, Schechter M, Tambussi G, Fidler S, Babiker A, Weber J, Kelleher AD, Phillips RE, Frater J. Immunological biomarkers predict HIV-1 viral rebound after treatment interruption. Nat Commun. 2015;6:8495. Epub 2015/10/10. doi: 10.1038/ncomms9495. PubMed PMID: 26449164; PubMed Central PMCID: PMCPMC4633715.

16. Li JZ, Etemad B, Ahmed H, Aga E, Bosch RJ, Mellors JW, Kuritzkes DR, Lederman MM, Para M, Gandhi RT. The size of the expressed HIV reservoir predicts timing of viral rebound after treatment interruption. AIDS. 2016;30(3):343-53. Epub 2015/11/21. doi: 10.1097/QAD.0000000000000953. PubMed PMID: 26588174; PubMed Central PMCID: PMCPMC4840470.

17. Assoumou L, Weiss L, Piketty C, Burgard M, Melard A, Girard PM, Rouzioux C, Costagliola D, group ASs. A low HIV-DNA level in peripheral blood mononuclear cells at antiretroviral treatment interruption predicts a higher probability of maintaining viral control. AIDS. 2015;29(15):2003-7. doi: 10.1097/QAD.0000000000000734. PubMed PMID: 26355572.

18. Williams JP, Hurst J, Stohr W, Robinson N, Brown H, Fisher M, Kinloch S, Cooper D, Schechter M, Tambussi G, Fidler S, Carrington M, Babiker A, Weber J, Koelsch KK, Kelleher AD, Phillips RE, Frater J, Investigators SP. HIV-1 DNA predicts disease progression and post-treatment virological control. eLife. 2014;3:e03821. doi: 10.7554/eLife.03821. PubMed PMID: 25217531; PubMed Central PMCID: PMC4199415.

19. Kumar N, Chahroudi A, Silvestri G. Animal models to achieve an HIV cure. Curr Opin HIV AIDS. 2016;11(4):432-41. doi: 10.1097/COH.0000000000000290. PubMed PMID: 27152962; PubMed Central PMCID: PMC4922307.

20. Van Rompay KK, Abel K, Lawson JR, Singh RP, Schmidt KA, Evans T, Earl P, Harvey D, Franchini G, Tartaglia J, Montefiori D, Hattangadi S, Moss B, Marthas ML. Attenuated poxvirus-based simian immunodeficiency virus (SIV) vaccines given in infancy partially protect infant and juvenile macaques against repeated oral challenge with virulent SIV. J Acquir Immune Defic Syndr. 2005;38(2):124-34. Epub 2005/01/27. PubMed PMID: 15671796.

21. Mavigner M, Habib J, Deleage C, Rosen E, Mattingly C, Bricker K, Kashuba A, Amblard F, Schinazi RF, Jean S, Cohen J, McGary C, Paiardini M, Wood MP, Sodora DL, Silvestri G, Estes J, Chahroudi A. Simian Immunodeficiency Virus Persistence in Cellular and Anatomic Reservoirs in Antiretroviral Therapy-Suppressed Infant Rhesus Macaques. Journal of virology. 2018;92(18). doi: 10.1128/JVI.00562-18. PubMed PMID: 29997216; PubMed Central PMCID: PMC6146711.

22. Li H, Wang S, Kong R, Ding W, Lee FH, Parker Z, Kim E, Learn GH, Hahn P, Policicchio B, Brocca-Cofano E, Deleage C, Hao X, Chuang GY, Gorman J, Gardner M, Lewis MG, Hatziioannou T, Santra S, Apetrei C, Pandrea I, Alam SM, Liao HX, Shen X, Tomaras GD, Farzan M, Chertova E, Keele BF, Estes JD, Lifson JD, Doms RW, Montefiori DC, Haynes BF, Sodroski JG, Kwong PD, Hahn BH, Shaw GM. Envelope residue 375 substitutions in simian-human immunodeficiency viruses enhance CD4 binding and replication in rhesus macaques. Proceedings of the National Academy of Sciences of the United States of America. 2016;113(24):E3413-22. doi:

10.1073/pnas.1606636113. PubMed PMID: 27247400; PubMed Central PMCID: PMC4914158.

23. Bar KJ, Coronado E, Hensley-McBain R, O'Connor MA, Osborn J, Miller C, Gott TM, Wangari S, Iwayama N, Ahrens CY, Smedley J, Moats C, Lynch RM, Haddad EK, Haigwood NL, Fuller DH, Shaw GM, Klatt NR, Manuzak J. SHIV.CH505 infection of rhesus macaques results in persistent viral replication and induces intestinal immunopathology. J Virol, in press.

24. Zhang ZQ, Fu TM, Casimiro DR, Davies ME, Liang X, Schleif WA, Handt L, Tussey L, Chen M, Tang A, Wilson KA, Trigona WL, Freed DC, Tan CY, Horton M, Emini EA, Shiver JW. Mamu-A*01 allele-mediated attenuation of disease progression in simian-human immunodeficiency virus infection. Journal of virology. 2002;76(24):12845-54. PubMed PMID: 12438610; PubMed Central PMCID: PMC136722.

25. Chen S, Lai C, Wu X, Lu Y, Han D, Guo W, Fu L, Andrieu JM, Lu W. Variability of bio-clinical parameters in Chinese-origin Rhesus macaques infected with simian immunodeficiency virus: a nonhuman primate AIDS model. PloS one. 2011;6(8):e23177. doi: 10.1371/journal.pone.0023177. PubMed PMID: 21850259; PubMed Central PMCID: PMC3151272.

26. Nelson AN, Goswami R, Dennis M, Tu J, Mangan RJ, Saha PT, Cain DW, Curtis AD, Shen X, Shaw GM, Bar K, Hudgens M, Pollara J, De Paris K, Van Rompay KKA, Permar SR. SHIV.CH505-infected infant and adult rhesus macaques exhibit similar HIV Env-specific antibody kinetics, despite distinct T-follicular helper (Tfh) and germinal center B cell landscapes. Journal of virology. 2019. doi: 10.1128/JVI.00168-19. PubMed PMID: 31092583.

778 27. Zanchetta M, Anselmi A, Vendrame D, Rampon O, Giaquinto C, Mazza A,
779 Accapezzato D, Barnaba V, De Rossi A. Early therapy in HIV-1-infected children: effect
780 on HIV-1 dynamics and HIV-1-specific immune response. Antiviral therapy.
781 2008;13(1):47-55. PubMed PMID: 18389898.
782 28. Roider JM, Muenchhoff M, Goulder PJ. Immune activation and paediatric HIV-1
783 disease outcome. Curr Opin HIV AIDS. 2016;11(2):146-55. Epub 2015/12/19. doi:
784 10.1097/COH.0000000000000231. PubMed PMID: 26679413; PubMed Central PMCID:
785 PMCPMC4745133.
786 29. Eudailey JA, Dennis ML, Parker ME, Phillips BL, Huffman TN, Bay CP, Hudgens
787 MG, Wiseman RW, Pollara JJ, Fouda GG, Ferrari G, Pickup DJ, Kozlowski PA, Van
788 Rompay KKA, De Paris K, Permar SR. Maternal HIV-1 Env Vaccination for Systemic
789 and Breast Milk Immunity To Prevent Oral SHIV Acquisition in Infant Macaques.
790 mSphere. 2018;3(1). doi: 10.1128/mSphere.00505-17. PubMed PMID: 29359183;
791 PubMed Central PMCID: PMC5760748.
792 30. Baan E, de Ronde A, Stax M, Sanders RW, Luchters S, Vyankandondera J,
793 Lange JM, Pollakis G, Paxton WA. HIV-1 autologous antibody neutralization associates
794 with mother to child transmission. PloS one. 2013;8(7):e69274. doi:
795 10.1371/journal.pone.0069274. PubMed PMID: 23874931; PubMed Central PMCID:
796 PMC3714266.
797 31. Mellors JW, Rinaldo CR, Jr., Gupta P, White RM, Todd JA, Kingsley LA.
798 Prognosis in HIV-1 infection predicted by the quantity of virus in plasma. Science.
799 1996;272(5265):1167-70. PubMed PMID: 8638160.

800 32. Milligan C, Richardson BA, John-Stewart G, Nduati R, Overbaugh J. Passively
801 acquired antibody-dependent cellular cytotoxicity (ADCC) activity in HIV-infected infants
802 is associated with reduced mortality. Cell Host Microbe. 2015;17(4):500-6. Epub
803 2015/04/10. doi: 10.1016/j.chom.2015.03.002. PubMed PMID: 25856755; PubMed
804 Central PMCID: PMCPMC4392343.
805 33. Frater J, Ewings F, Hurst J, Brown H, Robinson N, Fidler S, Babiker A, Weber J,
806 Porter K, Phillips RE, Investigators ST. HIV-1-specific CD4(+) responses in primary HIV-
807 1 infection predict disease progression. AIDS. 2014;28(5):699-708. doi:
808 10.1097/QAD.0000000000000130. PubMed PMID: 24549145.
809 34. van Rompay KK, Dailey PJ, Tarara RP, Canfield DR, Aguirre NL, Cherrington
810 JM, Lamy PD, Bischofberger N, Pedersen NC, Marthas ML. Early short-term 9-[2-(R)-
811 (phosphonomethoxy)propyl]adenine treatment favorably alters the subsequent disease
812 course in simian immunodeficiency virus-infected newborn Rhesus macaques. Journal
813 of virology. 1999;73(4):2947-55. Epub 1999/03/12. PubMed PMID: 10074144; PubMed
814 Central PMCID: PMCPMC104054.
815 35. Borducchi EN, Liu J, Nkolola JP, Cadena AM, Yu WH, Fischinger S, Broge T,
816 Abbink P, Mercado NB, Chandrashekar A, Jetton D, Peter L, McMahan K, Moseley ET,
817 Bekerman E, Hesselgesser J, Li W, Lewis MG, Alter G, Geleziunas R, Barouch DH.
818 Antibody and TLR7 agonist delay viral rebound in SHIV-infected monkeys. Nature.
819 2018;563(7731):360-4. Epub 2018/10/05. doi: 10.1038/s41586-018-0600-6. PubMed
820 PMID: 30283138; PubMed Central PMCID: PMCPMC6237629.
821 36. Buonaguro L, Tornesello ML, Buonaguro FM. Human immunodeficiency virus
822 type 1 subtype distribution in the worldwide epidemic: pathogenetic and therapeutic

implications. Journal of virology. 2007;81(19):10209-19. doi: 10.1128/JVI.00872-07. PubMed PMID: 17634242; PubMed Central PMCID: PMC2045484.

37. Himes JE, Goswami R, Mangan RJ, Kumar A, Jeffries TL, Jr., Eudailey JA, Heimsath H, Nguyen QN, Pollara J, LaBranche C, Chen M, Vandergrift NA, Peacock JW, Schiro F, Midkiff C, Ferrari G, Montefiori DC, Hernandez XA, Aye PP, Permar SR. Polyclonal HIV envelope-specific breast milk antibodies limit founder SHIV acquisition and cell-associated virus loads in infant rhesus monkeys. Mucosal immunology. 2018. doi: 10.1038/s41385-018-0067-7. PubMed PMID: 30115994.

38. Humbert M, Rasmussen RA, Song R, Ong H, Sharma P, Chenine AL, Kramer VG, Siddappa NB, Xu W, Else JG, Novembre FJ, Strobert E, O'Neil SP, Ruprecht RM. SHIV-1157i and passaged progeny viruses encoding R5 HIV-1 clade C env cause AIDS in rhesus monkeys. Retrovirology. 2008;5:94. Epub 2008/10/22. doi: 10.1186/1742-4690-5-94. PubMed PMID: 18928523; PubMed Central PMCID: PMCPMC2576354.

39. Subbarao S, Otten RA, Ramos A, Kim C, Jackson E, Monsour M, Adams DR, Bashirian S, Johnson J, Soriano V, Rendon A, Hudgens MG, Butera S, Janssen R, Paxton L, Greenberg AE, Folks TM. Chemoprophylaxis with tenofovir disoproxil fumarate provided partial protection against infection with simian human immunodeficiency virus in macaques given multiple virus challenges. The Journal of infectious diseases. 2006;194(7):904-11. Epub 2006/09/09. doi: 10.1086/507306. PubMed PMID: 16960777.

40. Muenchhoff M, Prendergast AJ, Goulder PJ. Immunity to HIV in Early Life. Front Immunol. 2014;5:391. Epub 2014/08/28. doi: 10.3389/fimmu.2014.00391. PubMed PMID: 25161656; PubMed Central PMCID: PMCPMC4130105.

41. Fouda GG, Cunningham CK, McFarland EJ, Borkowsky W, Muresan P, Pollara J, Song LY, Liebl BE, Whitaker K, Shen X, Vandergrift NA, Overman RG, Yates NL, Moody MA, Fry C, Kim JH, Michael NL, Robb M, Pitisuttithum P, Kaewkungwal J, Nitayaphan S, Rerks-Ngarm S, Liao HX, Haynes BF, Montefiori DC, Ferrari G, Tomaras GD, Permar SR. Infant HIV type 1 gp120 vaccination elicits robust and durable anti-V1V2 immunoglobulin G responses and only rare envelope-specific immunoglobulin A responses. The Journal of infectious diseases. 2015;211(4):508-17. Epub 2014/08/30. doi: 10.1093/infdis/jiu444. PubMed PMID: 25170104; PubMed Central PMCID: PMCPMC4318918.

42. McManus M, Henderson J, Gautam A, Brody R, Weiss ER, Persaud D, Mick E, Luzuriaga K, Investigators P. Quantitative Human Immunodeficiency Virus (HIV)-1 Antibodies Correlate With Plasma HIV-1 RNA and Cell-associated DNA Levels in Children on Antiretroviral Therapy. Clin Infect Dis. 2018. Epub 2019/01/23. doi: 10.1093/cid/ciy753. PubMed PMID: 30668843.

43. Li JZ, Brumme ZL, Brumme CJ, Wang H, Spritzler J, Robertson MN, Lederman MM, Carrington M, Walker BD, Schooley RT, Kuritzkes DR, Team ACTGAS. Factors associated with viral rebound in HIV-1-infected individuals enrolled in a therapeutic HIV-1 gag vaccine trial. The Journal of infectious diseases. 2011;203(7):976-83. doi: 10.1093/infdis/jiq143. PubMed PMID: 21402549; PubMed Central PMCID: PMC3068025.

44. Burbelo PD, Bayat A, Rhodes CS, Hoh R, Martin JN, Fromentin R, Chomont N, Hutter G, Kovacs JA, Deeks SG. HIV antibody characterization as a method to quantify reservoir size during curative interventions. The Journal of infectious diseases.

2014;209(10):1613-7. Epub 2013/11/30. doi: 10.1093/infdis/jit667. PubMed PMID: 24286982; PubMed Central PMCID: PMCPMC3997576.

45. McLinden RJ, Paris RM, Polonis VR, Close NC, Su Z, Shikuma CM, Margolis DM, Kim JH. Association of HIV neutralizing antibody with lower viral load after treatment interruption in a prospective trial (A5170). AIDS. 2012;26(1):1-9. Epub 2011/10/06. doi: 10.1097/QAD.0b013e32834d606e. PubMed PMID: 21971356.

46. Li JZ, Heisey A, Ahmed H, Wang H, Zheng L, Carrington M, Wrin T, Schooley RT, Lederman MM, Kuritzkes DR, Team AAS. Relationship of HIV reservoir characteristics with immune status and viral rebound kinetics in an HIV therapeutic vaccine study. AIDS. 2014;28(18):2649-57. Epub 2014/09/26. doi: 10.1097/QAD.0000000000000478. PubMed PMID: 25254301; PubMed Central PMCID: PMCPMC4267919.

47. Dennis M, Eudailey J, Pollara J, McMillan AS, Cronin KD, Saha PT, Curtis AD, Hudgens MG, Fouda GG, Ferrari G, Alam M, Van Rompay KKA, De Paris K, Permar S, Shen X. Co-administration of CH31 broadly neutralizing antibody does not affect development of vaccine-induced anti-HIV-1 envelope antibody responses in infant Rhesus macaques. Journal of virology. 2018. Epub 2018/12/14. doi: 10.1128/JVI.01783-18. PubMed PMID: 30541851.

48. Cline AN, Bess JW, Piatak M, Jr., Lifson JD. Highly sensitive SIV plasma viral load assay: practical considerations, realistic performance expectations, and application to reverse engineering of vaccines for AIDS. Journal of medical primatology. 2005;34(5-6):303-12. doi: 10.1111/j.1600-0684.2005.00128.x. PubMed PMID: 16128925.

891 49. Del Prete GQ, Smedley J, Macallister R, Jones GS, Li B, Hattersley J, Zheng J,
892 Piatak M, Jr., Keele BF, Hesselgesser J, Geleziunas R, Lifson JD. Short
893 Communication: Comparative Evaluation of Coformulated Injectable Combination
894 Antiretroviral Therapy Regimens in Simian Immunodeficiency Virus-Infected Rhesus
895 Macaques. AIDS research and human retroviruses. 2016;32(2):163-8. doi:
896 10.1089/AID.2015.0130. PubMed PMID: 26150024; PubMed Central PMCID:
897 PMC4761795.
898 50. Evans DT, Knapp LA, Jing P, Mitchen JL, Dykhuizen M, Montefiori DC, Pauza
899 CD, Watkins DI. Rapid and slow progressors differ by a single MHC class I haplotype in
900 a family of MHC-defined rhesus macaques infected with SIV. Immunol Lett. 1999;66(1-
901 3):53-9. Epub 1999/04/15. PubMed PMID: 10203034.
902 51. Knapp LA, Lehmann E, Piekarczyk MS, Urvater JA, Watkins DI. A high frequency
903 of Mamu-A*01 in the rhesus macaque detected by polymerase chain reaction with
904 sequence-specific primers and direct sequencing. Tissue Antigens. 1997;50(6):657-61.
905 Epub 1998/02/11. PubMed PMID: 9458122.
906 52. Montefiori DC. Measuring HIV neutralization in a luciferase reporter gene assay.
907 Methods in molecular biology. 2009;485:395-405. doi: 10.1007/978-1-59745-170-3_26.
908 PubMed PMID: 19020839.
909 53. Sarzotti-Kelsoe M, Bailer RT, Turk E, Lin CL, Bilska M, Greene KM, Gao H, Todd
910 CA, Ozaki DA, Seaman MS, Mascola JR, Montefiori DC. Optimization and validation of
911 the TZM-bl assay for standardized assessments of neutralizing antibodies against HIV-
912 1. Journal of immunological methods. 2014;409:131-46. doi: 10.1016/j.jim.2013.11.022.
913 PubMed PMID: 24291345; PubMed Central PMCID: PMC4040342.

914 54. Pollara J, Hart L, Brewer F, Pickeral J, Packard BZ, Hoxie JA, Komoriya A,
915 Ochsenbauer C, Kappes JC, Roederer M, Huang Y, Weinhold KJ, Tomaras GD,
916 Haynes BF, Montefiori DC, Ferrari G. High-throughput quantitative analysis of HIV-1
917 and SIV-specific ADCC-mediating antibody responses. Cytometry Part A : the journal of
918 the International Society for Analytical Cytology. 2011;79(8):603-12. doi:
919 10.1002/cyto.a.21084. PubMed PMID: 21735545; PubMed Central PMCID:
920 PMC3692008.
921 55. Kumar A, Smith CEP, Giorgi EE, Eudailey J, Martinez DR, Yusim K, Douglas AO,
922 Stamper L, McGuire E, LaBranche CC, Montefiori DC, Fouda GG, Gao F, Permar SR.
923 Infant transmitted/founder HIV-1 viruses from peripartum transmission are neutralization
924 resistant to paired maternal plasma. PLoS pathogens. 2018;14(4):e1006944. doi:
925 10.1371/journal.ppat.1006944. PubMed PMID: 29672607; PubMed Central PMCID:
926 PMC5908066.
927 56. Gouy M, Guindon S, Gascuel O. SeaView version 4: A multiplatform graphical
928 user interface for sequence alignment and phylogenetic tree building. Molecular biology
929 and evolution. 2010;27(2):221-4. doi: 10.1093/molbev/msp259. PubMed PMID:
930 19854763.
931 57. Tamura K, Stecher G, Peterson D, Filipski A, Kumar S. MEGA6: Molecular
932 Evolutionary Genetics Analysis version 6.0. Molecular biology and evolution.
933 2013;30(12):2725-9. Epub 2013/10/18. doi: 10.1093/molbev/mst197. PubMed PMID:
934 24132122; PubMed Central PMCID: PMCPMC3840312.
935 58. Curtis AD, 2nd, Walter KA, Nabi R, Jensen K, Dwivedi A, Pollara J, Ferrari G,
936 Van Rompay KKA, Amara RR, Kozlowski PA, De Paris K. Oral Coadministration of an

Intramuscular DNA/Modified Vaccinia Ankara Vaccine for Simian Immunodeficiency Virus Is Associated with Better Control of Infection in Orally Exposed Infant Macaques. AIDS research and human retroviruses. 2018. doi: 10.1089/AID.2018.0180. PubMed PMID: 30303405.

59. Amedee AM, Phillips B, Jensen K, Robichaux S, Lacour N, Burke M, Piatak M, Jr., Lifson JD, Kozlowski PA, Van Rompay KKA, De Paris K. Early Sites of Virus Replication After Oral SIVmac251 Infection of Infant Macaques: Implications for Pathogenesis. AIDS research and human retroviruses. 2018;34(3):286-99. doi: 10.1089/AID.2017.0169. PubMed PMID: 29237287; PubMed Central PMCID: PMC5863100.

60. R: A language and environment for statistical computing. R Foundation for Statistical Computing, Vienna, Austria. R Core Team 2018.

960 **FIGURE LEGENDS.**

961

962 **Figure 1: SHIV.CH505.375H.dCT replication kinetics prior to and following ATI in**
963 **infant RMs. (A)** Schematic representation of SHIV.CH505.375H.dCT infection (0-12
964 weeks), ART (12-20 weeks) and ATI (20-28 weeks) in infant RMs. Blood samples were
965 collected at weekly intervals throughout the study and peripheral lymph nodes (LN)
966 were collected at 12 w.p.i and on ART (20 w.p.i) **(B)** Kinetics of plasma SHIV RNA over
967 28 weeks was measured by qRT-PCR. **(C)** Peripheral lymph nodes from RMs on ART
968 (20 w.p.i) were collected, and naïve, memory and Tfh CD4+ T cell-associated SHIV
969 DNA was estimated by qPCR. **(D)** Cell-associated SHIV DNA (CA-SHIV DNA) and **(E)**
970 cell-associated SHIV RNA (CA-SHIV RNA) per million CD4+ T cells in the peripheral
971 blood was monitored by ddPCR in the infant RMs pre-ART (6 w.p.i) and on ART (18
972 w.p.i). The sensitivity of the ddPCR assay was detection of 1 SHIV gag copy in 10,000
973 CD4+ T cells. Therefore, only those animals that had ≥10,000 CD4+ T cells at a
974 particular time point, were included in the analysis. Each symbol represents an
975 individual animal. Yellow and grey boxes represent duration of ART (week 12-20) and
976 duration of ATI (week 20-28), respectively. Medians are indicated as horizontal lines on
977 the dot plots. Infants with plasma VL<15 copies/mL at 12 w.p.i has been represented
978 with open symbols.

979

980 **Figure 2: Tissue-associated infectious viral loads upon ATI, in mononuclear cells**
981 **isolated from PBMCs, lymphoid and GI tissues of orally infected infant RMs (A)**
982 Tissue-associated infectious SHIV.CH505.375H.dCT titers measured through tissue

mononuclear cell coculture with Tzm-bl reporter cells. Reported titers represents the estimated minimum number of mononuclear cells per 10^4 mononuclear cells required to yield detectable infection of 50% Tzm-bl cells (CID_{50}). **(B)** CD4+ T cell-associated proviral DNA and **(C)** CD4+ T cell-associated viral RNA loads at necropsy (28 w.p.i) reported as copy number/million CD4+ T cells in PBMCs, lymphoid and GI tissue mononuclear cells. Each symbol represents one individual animal. Medians are indicated as horizontal lines on the dot plots. Infants with plasma VL<15 copies/mL at 12 w.p.i has been represented with open symbols. The sensitivity of the ddPCR assay was detection of 1 SHIV gag copy in 10,000 CD4+ T cells. Therefore, only those animals that had ≥10,000 CD4+ T cells at a particular time point, were included in the analysis. **(D)** Tonsil and colon sections from the SHIV.CH505.375H.dCT infected infant RM that demonstrated highest peak plasma VL post-rebound (20,000 vRNA copies/mL plasma). Tissue sections were stained with the nuclear marker DAPI (dark blue) to identify cells, and with antibodies specific for CD3 (green) and CD20 (red). Virally-infected cells were identified by *in-situ* hybridization (cyan). To better visualize the virally-infected cells, we magnified a specific region (white box) in each image. Each panel consists of a larger image with the overlay of all markers and 4 smaller side panels of the same field for each individual channel. Arrow colors correspond to the indicated marker. The large image has a scale bar in the lower right corner.

Figure 3: SHIV.CH505.375H.dCT replication kinetics prior to and following ATI in adult RMs. (A) Schematic representation of SHIV.CH505.375H.dCT infection (0-12 weeks), ART (12-24 weeks) and ATI (24-32 weeks) in adult RMs. Blood samples were

collected at weekly intervals throughout the study and peripheral lymph nodes (LN) were collected at 12 w.p.i and after 8 weeks of ART (20 w.p.i) **(B)** Kinetics of plasma SHIV RNA over 32 weeks was measured by qRT-PCR. **(C)** Peripheral lymph nodes from macaques on ART (20 w.p.i) were collected, and naïve, memory and Tfh CD4+ T cell-associated SHIV DNA was estimated by qPCR. **(D)** Cell-associated SHIV DNA (CA-SHIV DNA) and **(E)** Cell-associated SHIV RNA (CA-SHIV RNA) from CD4+ T cells of peripheral blood pre-ART (6 w.p.i for DNA and 12 w.p.i for RNA) and on-ART (18 w.p.i) was monitored by ddPCR. The sensitivity of the ddPCR assay was detection of 1 SHIV gag copy in 10,000 CD4+ T cells. Therefore, only those animals that had ≥10,000 CD4+ T cells at a particular time point, were included in the analysis. Each symbol represents an individual animal. Yellow and grey boxes represent duration of ART (week 12-24) and duration of ATI (week 24-32), respectively. Medians are indicated as horizontal lines on the dot plots.

Figure 4: Tissue-associated infectious virus load upon ATI, in mononuclear cells isolated from PBMCs, lymphoid and GI tissues of adult RMs intravenously infected with SHIV.CH505.375H.dCT (A) Tissue-associated infectious SHIV.CH505.375H.dCT titers measured through tissue mononuclear cell coculture with Tzm-bl reporter cells. Reported titers represents the estimated minimum number of mononuclear cells per 10^4 mononuclear cells required to yield detectable infection of 50% Tzm-bl cells (CID_{50}). **(B)** CD4+ T cell-associated proviral DNA and **(C)** Viral RNA loads reported as copy number/million CD4+ T cells in PBMCs, lymphoid and GI tissue mononuclear cells. Each symbol represents one individual monkey at necropsy (week

32 pi). Medians are indicated as horizontal lines on the dot plots. **(D)** Tonsil and colon sections from the SHIV.CH505.375H.dCT infected adult RM (39950) that demonstrated highest peak plasma VL post-rebound (13000 vRNA copies/mL plasma). Tissue sections were stained with the nuclear marker DAPI (dark blue) to identify cells, and with antibodies specific for CD3 (green) and CD20 (red). Virally-infected cells were identified by *in-situ* hybridization (cyan). Each panel consists of a larger image with the overlay of all markers and 4 smaller side panels of the same field for each individual channel. Arrow colors correspond to the indicated marker. The large image has a scale bar in the lower right corner.

Figure 5. Phylogenetic tree analysis of the *env* gene sequences obtained from pre-ART and post-ATI plasma of infant and adult RM demonstrating highest peak plasma VL post-rebound. Standard SGA techniques were used to analyze the *env* gene from pre-ART and post-ATI samples of infants and adult RMs with highest peak rebound plasma VL. Phylogenetic tree representing viral Env diversity in **(A)** infant 46352 and **(B)** adult 39950.

Figure 6: Magnitude and kinetics of humoral responses to acute SHIV.CH505.375H.dCT infection, during ART and ATI in RMs. Plasma from infant and adult rhesus macaques were analyzed for **(A)** HIV CH505 gp120 IgG response **(B)** blocking of soluble CD4-gp120 interactions **(C)** tier-1 neutralization response against MW965 **(D)** neutralization response against CH505 T/F, and **(E)** ADCC titer against CH505 gp120-coated target cells. Red symbols represent infant RMs and blue symbols

represent adult RMs. Each symbol represents an individual macaque. Yellow and grey boxes represent duration of ART and duration of ATI in the RMs, respectively. Infants with plasma VL<15 copies/mL at 12 w.p.i has been represented with open symbols. P values were calculated using Wilcoxon signed rank test.

Figure 7: CD4+ T cell activation and plasma inflammatory responses in SHIV.CH505.375H.dCT infected infant and adult RMs. Absolute counts per ml blood of **(A)** activated (CD69+, HLADR+) CD4+ T cells and **(B)** proliferating (Ki67+ CD4+) and exhausted (PD-1+) CD4+ T cells. Red symbol represents infant RMs and blue symbols represents adult RMs. Each symbol represents one animal. Yellow and grey boxes represent duration of ART and duration of ATI, respectively. **(C)** Plasma from infected infant and adult RMs were analyzed by multiplexed luminex assay for expression of cytokines before ART (week 12) and 8 weeks on ART (week 20). Heat map represents fold change of each analyte over pre-infection plasma levels. Infants with plasma VL<15 copies/mL at 12 w.p.i has been represented with open symbols. P values were calculated using Wilcoxon signed rank test.

SUPPLEMENTAL MATERIALS.

Figure S1: Proportions of CD4+ T cells in blood, lymph nodes and gut-associated tissues of SHIV.CH505.375H.dCT infected infants and adult RMs. (A) Frequencies of PBMC-CD4+ T cells in SHIV.CH505.375H.dCT infected infant and adult RMs through 28 w.p.i and 32 w.p.i, respectively. **(B)** Proportions of CD4+ T cells of CD3+ T cells in PBMC, oral and gut-associated lymphoid tissues, and spleen of infected infant RMs at necropsy (28 w.p.i) and adult RMs at necropsy (32 w.p.i). Red symbols represent infants and blue symbols represent adults. Each symbol represents one animal. Yellow and grey boxes represent duration of ART and duration of ATI, respectively. Infants with plasma VL<15 copies/mL at 12 w.p.i has been represented with open symbols.

Figure S2: Tissue-associated infectious viral levels in RMs infected with SHIV.CH505.375H.dCT. Mononuclear cells isolated from tissues of **(A)** infant and **(B)** adult RMs infected with SHIV.CH505.375H.dCT were serially diluted and co-cultured with Tzm-bl reporter cells for 72 hrs, followed by luminescent detection of tissue-associated SHIV infectivity in relative luminescence units (RLU). The RLU limit of detection for positive tissue-associated SHIV infection (dashed line) was defined as 2.5 times the mean maximum RLU elicited form Tzm-bl cells (n=10 independent assays) in the co-culture assay.

Figure S3: Specificity of Env-IgG responses before- and on-ART in SHIV.CH505.375H.dCT infected RMs. Plasma IgG specificity against a panel of HIV

Env linear and conformational epitopes pre ART (12 w.p.i) and on ART (20 w.p.i) in SHIV.C.CH505 infected **(A)** infant and **(B)** adult RMs. Heat maps represents mean fluorescence intensity (MFI) of IgG binding to each epitope.

Figure S4: Flow cytometry gating strategy for T cell phenotyping and sorting. For T cell phenotyping, CD4+ T cells and CD8+ T cells were positively selected from the PBMCs by sequential selection of forward and side scatter singlets, lymphocytes, viable cells, CD16-CD14- (Monocytes/macrophages) cells and CD3+ cells (T cells). CD4+ T cells were further analyzed for expression of activation markers HLA-DR and CD69; proliferation marker Ki67 and exhaustion markers PD-1. For sorting CD4+ T cells, CD4+ T cells were positively selected from lymph node-associated mononuclear cells by sequential selection of forward scatter singlets, lymphocytes and $CD3^{+}$ T cells. Tfh cells ($CXCR5^{hi}$ $PD\text{-}1^{hi}$), naïve CD4+ T cells (CD95- CD28+ CD45RA+ CCR7+) and memory CD4+ T cells (CD95+ CD28+ CD45RA- CCR7+) were sorted from CD4+ T cells.

Table S1. MHC class I genotype of infant and adult RMs.

Table S2. Antibodies used for T cell phenotyping, CD4+ T cell sorting and *in situ* hybridization (ISH).

Table S3. Primers and probes used for the assays.

Table 1. SHIV.CH505.375H.dCT infected rhesus macaques, weeks of challenges to infection, age at infection, sex, time to viral control post-ART and time to viral rebound post-ATI.

Animal Age	Animal ID	Challenges to infection (wk)	Age at infection[a]	Sex[b]	Pre- ART control[c,e]	Time to viral control post-ART (wk)[d,f]	Viral rebound post ATI[c,g]	Time to viral rebound post-ATI (wk)[d]	Post- rebound control[c,d,h]
Infant	46357	1	5	M	N	1	Y	3	N
	46346	2	9	F	N	1	Y	6	Y
	46352	2	9	F	N	4	Y	1	N
	46359	3	10	F	Y	N/A	N	N/A	N/A
	46367	7	14	M	Y	N/A	Y	4	Y
	46380	4	11	F	N	1	Y	3	N
Adult	39472	1	8	F	N	1	N	N/A	N/A
	43068	1	5	F	N	1	N	N/A	N/A
	43268	1	4	F	N	1	Y	3	N
	42368	1	5	F	N	1	Y	3	Y
	39950	1	8	F	N	4	Y	2	N
	38200	1	10	F	N	1	N	N/A	N/A

[a]Weeks in infants; years in adults

[b]M, male; F, female

[c]N, No; Y,Yes

[d]N/A, Not applicable

[e]Pre ART control: plasma VL≤15 copies/mL at ART start (12 w.p.i)

[f]Viral control post ART: plasma VL≤15 copies/mL after ART start

[g]Viral rebound: Plasma VL≥10X detection limit of the assay (150 copies of vRNA/mL plasma) post ART discontinuation

[h]Post-rebound control: Plasma VL≤15 copies/mL after 8 weeks post-ATI, in monkeys showing viral rebound.

Table 2. Virologic and immunologic correlates of time to viral rebound, with adjustment for age.

Variables	HR (95% CI)	Unadjusted p value	Adjusted p value
Pre-selected Variables			
Plasma VL at ART start[a]	2.2 (1.24-3.95)	**0.008**	NA
ADCC antibody titer on ART[a]	1.9 (1.05-3.45)	**0.034**	NA
CD4+ CD69+ T cells on ART[b]	0.82 (0.26-2.56)	0.727	NA
CH505 T/F neutralizing antibody titer at ART start[a]	2.1 (0.82-5.57)	0.119	NA
Exploratory Variables			
(a) Virologic and humoral responses			
Peak plasma VL[a]	1.39 (0.86-2.27)	0.182	0.364
CH505 gp120-specific IgG pre ART[a]	4.61 (1.38-15.42)	**0.0131**	0.066
CH505 gp120-specific IgG on ART[a]	6.06 (1.33-27.54)	**0.0197**	0.066
Tier-1 MW965 neutralizing antibody pre-ART[a]	4.12 (1.42-11.96)	**0.00926**	0.066
sCD4 blocking antibodies pre-ART[c]	1.07 (1-1.13)	**0.0402**	0.1
(b) CD4+ T cell phenotypes and inflammatory responses			
CD4+ T pre-ART[b]	0.97 (0.86-1.1)	0.66	0.81
CD4+ T on ART[b]	0.99 (0.9-1.09)	0.77	0.82
HLADR+ CD4+ T on ART[b]	1 (1-1)	0.71	0.81
Ki67+ CD4+ T on ART[b]	1 (0.98-1.05)	0.4	0.8
PD-1+ CD4+ T on ART[b]	1 (1-1)	0.32	0.8
G-CSF on ART[b]	1.1 (0.91-1.28)	0.36	0.8
IL-12 on ART[d]	1.1 (0.96-1.36)	0.13	0.8
IL-15 on ART[d]	0.77 (0.4-1.5)	0.45	0.8
IL-18 on ART[d]	0.97 (0.93-1.01)	0.15	0.8
IL-1RA on ART[d]	1 (0.99-1.01)	0.71	0.81
IL-8 on ART[d]	1 (1-1)	0.97	0.97
MCP-1 on ART[d]	1 (0.99-1.02)	0.34	0.8
MIP1a on ART[d]	0.68 (0.3-1.57)	0.37	0.8
TNFa on ART[d]	0.91 (0.79-1.04)	0.17	0.8
VEGF on ART[d]	0.97 (0.86-1.1)	0.64	0.81
SCD40L on ART[d]	1 (1-1)	0.7	0.81

Values expressed as [a]Log_{10}; [b]Absolute counts/nL of blood; [c]Percentages; [d]Concentrations

HR: Hazard ratio; CI: Confidence Interval; NA: Not applicable since multiple adjustment was not performed on pre-selected parameters.

Table 3. Virologic and immunologic correlates of time to viral rebound in each age group.

Variables	Infant			Adult		
	Kendall's Tau	Unadjusted p value	Adjusted p value	Kendall's Tau	Unadjusted p value	Adjusted p value
Pre-selected Variables						
Plasma VL at ART start[a]	-0.786	**0.032**	NA	-0.886	**0.022**	NA
ADCC antibody titer on ART[a]	-0.414	0.251	NA	-0.701	0.064	NA
CD4+ CD69+ T cells on ART[b]	0.276	0.444	NA	-0.078	0.837	NA
CH505 T/F neutralizing antibody titer at ART start[a]	-0.54	0.152	NA	-0.322	0.404	NA
Exploratory Variables						
(a) Virologic and humoral responses						
Peak plasma VL[a]	0	1	1	-0.856	**0.024**	**0.04**
CH505 gp120-specific IgG pre ART[a]	-0.69	**0.056**	0.14	-0.856	**0.024**	**0.04**
CH505 gp120-specific IgG on ART[a]	-0.69	**0.056**	0.14	-0.701	0.064	0.08
Tier-1 MW965 neutralizing antibody pre-ART[a]	-0.552	0.126	0.158	-0.856	**0.024**	**0.04**
sCD4 blocking antibodies pre-ART[c]	-0.552	0.126	0.158	-0.545	0.15	0.15
(b) CD4+ T cell phenotypes and inflammatory responses						
CD4+ T pre-ART[b]	0.138	0.702	0.936	0.078	0.837	0.837
CD4+ T on ART[b]	0	1	1	0.234	0.537	0.781
HLADR+ CD4+ T on ART[b]	0.276	0.444	0.936	-0.078	0.837	0.837
Ki67+ CD4+ T on ART[b]	-0.276	0.444	0.936	0.078	0.837	0.837
PD-1+ CD4+ T on ART[b]	0.138	0.702	0.936	0.545	0.15	0.781
G-CSF on ART[b]	0.357	0.33	0.936	-0.418	0.289	0.781
IL-12 on ART[d]	-0.357	0.33	0.936	-0.261	0.511	0.781
IL-15 on ART[d]	-0.138	0.702	0.936	0.322	0.404	0.781
IL-18 on ART[d]	0.552	0.126	0.936	0.405	0.343	0.781
IL-1RA on ART[d]	0.138	0.702	0.936	0.389	0.304	0.781
IL-8 on ART[d]	0.138	0.702	0.936	0.078	0.837	0.837
MCP-1 on ART[d]	-0.414	0.251	0.936	-0.234	0.537	0.781
MIP1a on ART[d]	0.077	0.838	0.967	0.405	0.343	0.781
TNFa on ART[d]	0.357	0.33	0.936	0.234	0.537	0.781
VEGF on ART[d]	-0.071	0.846	0.967	0.087	0.827	0.837
SCD40L on ART[d]	0	1	1	-0.234	0.537	0.781

Values expressed as [a]Log_{10}; [b]Absolute counts/nL of blood; [c]Percentages; [d]Concentrations

NA: Not applicable since multiple adjustment was not performed on pre-selected parameters.

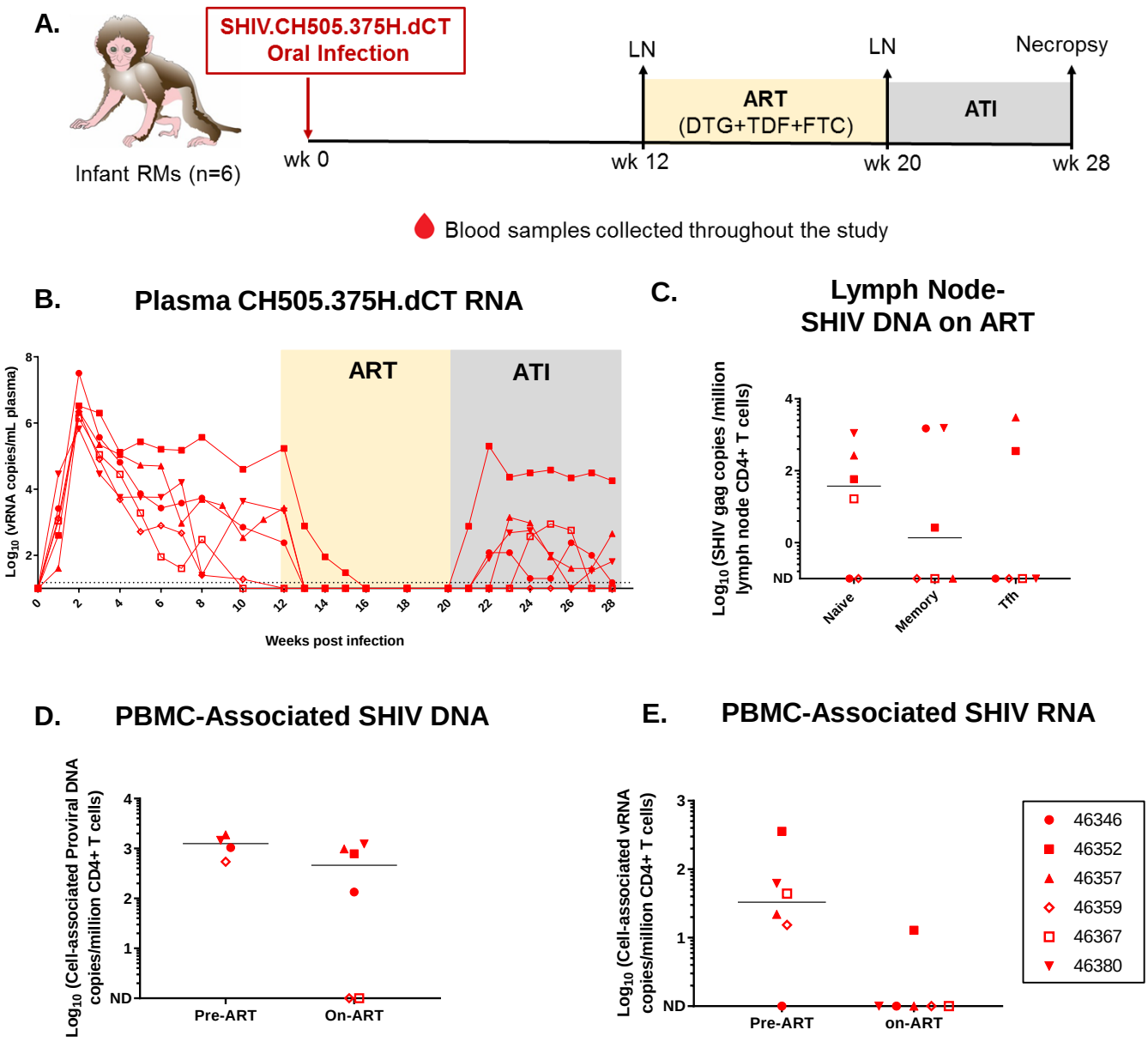

Figure 1: SHIV.CH505.375H.dCT replication kinetics prior to and following ATI in infant RMs. (A) Schematic representation of SHIV.CH505.375H.dCT infection (0-12 weeks), ART (12-20 weeks) and ATI (20-28 weeks) in infant RMs. Blood samples were collected at weekly intervals throughout the study and peripheral lymph nodes (LN) were collected at 12 w.p.i and on ART (20 w.p.i) **(B)** Kinetics of plasma SHIV RNA over 28 weeks was measured by qRT-PCR. **(C)** Peripheral lymph nodes from RMs on ART (20 w.p.i) were collected, and naïve, memory and Tfh CD4+ T cell-associated SHIV DNA was

estimated by qPCR. **(D)** Cell-associated SHIV DNA (CA-SHIV DNA) and **(E)** cell-associated SHIV RNA (CA-SHIV RNA) per million CD4+ T cells in the peripheral blood was monitored by ddPCR in the infant RMs pre-ART (6 w.p.i) and on ART (18 w.p.i). The sensitivity of the ddPCR assay was detection of 1 SHIV gag copy in 10,000 CD4+ T cells. Therefore, only those animals that had ≥10,000 CD4+ T cells at a particular time point, were included in the analysis. Each symbol represents an individual animal. Yellow and grey boxes represent duration of ART (week 12-20) and duration of ATI (week 20-28), respectively. Medians are indicated as horizontal lines on the dot plots. Infants with plasma VL<15 copies/mL at 12 w.p.i has been represented with open symbols.

A. **Tissue- associated infectious viral load 8 weeks post- ATI**

		46357	46346	46352	46359	46367	46380
Plasma	**SHIV RNA copies/ml**	450	<15	18000	<15	<15	65
Spleen	**50% Cellular Infectious Dose (CID_{50})***	>400	>400	2.0	>400	>400	>400
Mesenteric LN		30.8		3.5	>400	>400	400
Submandibular LN		10	>400	0.3	200	>400	11.7
Retropharyngeal LN					200		25
PBMC					>400	>400	>400
Ileum			>400	5.3	60.5		190

CID_{50} Key

	0-19
	20-49
	50-99
	100-200
	>200
	Tissue not available

***CID_{50}:** Number of mononuclear cells/10^4 mononuclear cells needed to yield detectable infection of 50% Tzm-bl cells.

B. **Tissue- Associated SHIV DNA 8 weeks post-ATI**

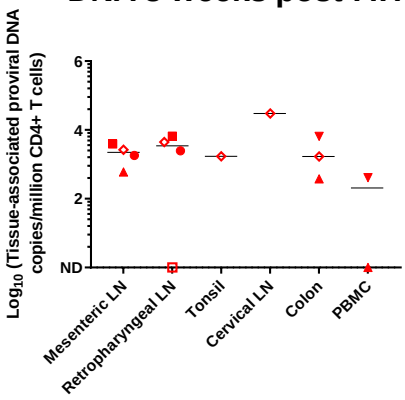

C. **Tissue- Associated SHIV RNA 8 weeks post-ATI**

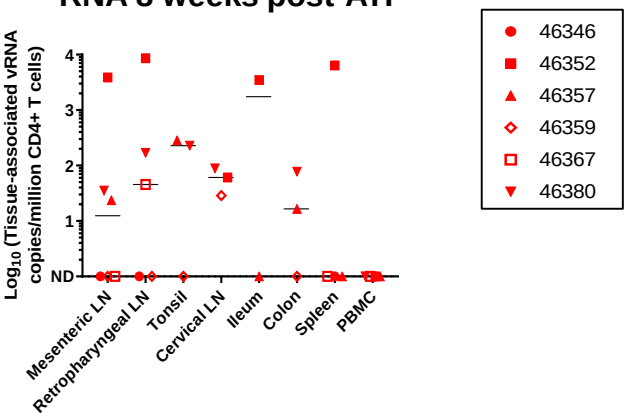

D. **46352-Tonsil**

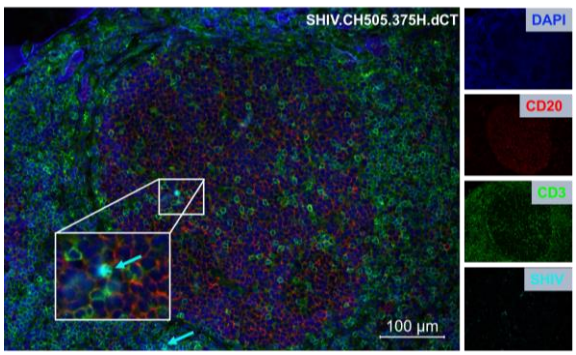

46352-Colon Lymphoid Aggregate

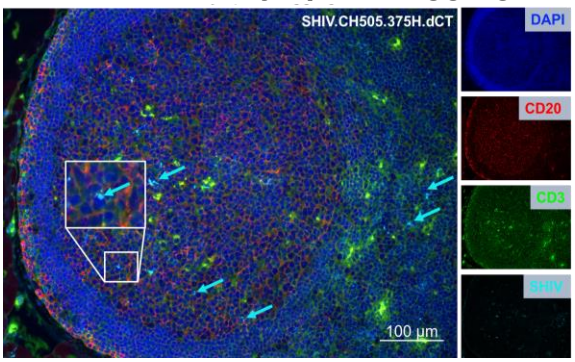

Figure 2: Tissue-associated infectious viral loads upon ATI, in mononuclear cells isolated from PBMCs, lymphoid and GI tissues of orally infected infant RMs (A) Tissue-associated infectious SHIV.CH505.375H.dCT titers measured through tissue mononuclear cell coculture with Tzm-bl reporter cells. Reported titers represents the estimated minimum number of mononuclear cells per 10^4 mononuclear cells required to yield detectable infection of 50% Tzm-bl cells (CID_{50}). **(B)** CD4+ T cell-associated proviral DNA and **(C)** CD4+ T cell-associated viral RNA loads at

necropsy (28 w.p.i) reported as copy number/million CD4+ T cells in PBMCs, lymphoid and GI tissue mononuclear cells. Each symbol represents one individual animal. Medians are indicated as horizontal lines on the dot plots. Infants with plasma VL<15 copies/mL at 12 w.p.i has been represented with open symbols. The sensitivity of the ddPCR assay was detection of 1 SHIV gag copy in 10,000 CD4+ T cells. Therefore, only those animals that had ≥10,000 CD4+ T cells at a particular time point, were included in the analysis. **(D)** Tonsil and colon sections from the SHIV.CH505.375H.dCT infected infant RM that demonstrated highest peak plasma VL post-rebound (20,000 vRNA copies/mL plasma). Tissue sections were stained with the nuclear marker DAPI (dark blue) to identify cells, and with antibodies specific for CD3 (green) and CD20 (red). Virally-infected cells were identified by *in-situ* hybridization (cyan). To better visualize the virally-infected cells, we magnified a specific region (white box) in each image. Each panel consists of a larger image with the overlay of all markers and 4 smaller side panels of the same field for each individual channel. Arrow colors correspond to the indicated marker. The large image has a scale bar in the lower right corner.

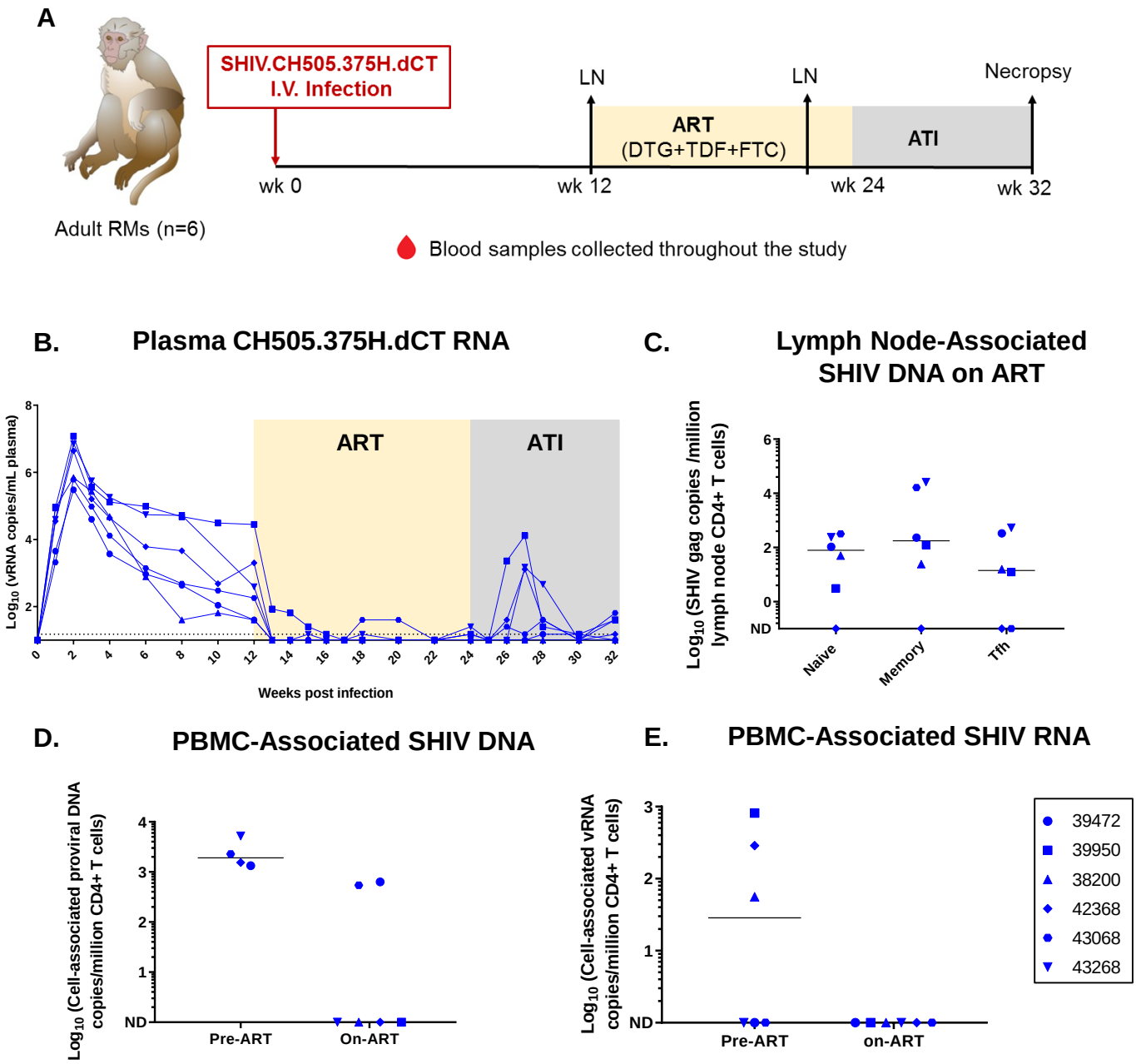

Figure 3: SHIV.CH505.375H.dCT replication kinetics prior to and following ATI in adult RMs. (A) Schematic representation of SHIV.CH505.375H.dCT infection (0-12 weeks), ART (12-24 weeks) and ATI (24-32 weeks) in adult RMs. Blood samples were collected at weekly intervals throughout the study and peripheral lymph nodes (LN) were collected at 12 w.p.i and after 8 weeks of ART (20 w.p.i) **(B)** Kinetics of plasma SHIV RNA over 32 weeks was measured by qRT-PCR.

(C) Peripheral lymph nodes from macaques on ART (20 w.p.i) were collected, and naïve, memory and Tfh CD4+ T cell-associated SHIV DNA was estimated by qPCR. **(D)** Cell-associated SHIV DNA (CA-SHIV DNA) and **(E)** Cell-associated SHIV RNA (CA-SHIV RNA) from CD4+ T cells of peripheral blood pre-ART (6 w.p.i for DNA and 12 w.p.i for RNA) and on-ART (18 w.p.i) was monitored by ddPCR. The sensitivity of the ddPCR assay was detection of 1 SHIV gag copy in 10,000 CD4+ T cells. Therefore, only those animals that had ≥10,000 CD4+ T cells at a particular time point, were included in the analysis. Each symbol represents an individual animal. Yellow and grey boxes represent duration of ART (week 12-24) and duration of ATI (week 24-32), respectively. Medians are indicated as horizontal lines on the dot plots.

A. **Tissue- associated infectious viral load 8 weeks post- ATI**

		39472	43068	43268	42368	39950	38200
Plasma	**SHIV RNA copies/ml**	<15	65	40	<15	40	<15
Spleen	**50% Cellular Infectious Dose (CID_{50})***	>400	>400	>400	>400	>400	>400
Mesenteric LN		>400	80	400	>400	200	>400
Submandibular LN		20	50	66.7	200	23.5	>400
Retropharyngeal LN		13	40	80	200	25	100
PBMC		>400	>400	>400	>400	>400	>400
Ileum		250				>400	>400

CID_{50} Key	
	0-19
	20-49
	50-99
	100-200
	>200
	Tissue not available

***CID_{50}:** Number of mononuclear cells/10^4 mononuclear cells needed to yield detectable infection of 50% Tzm-bl cells.

B.

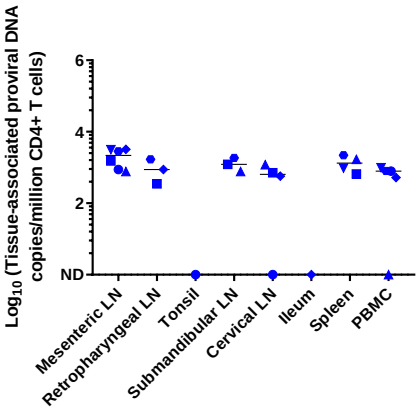

C.

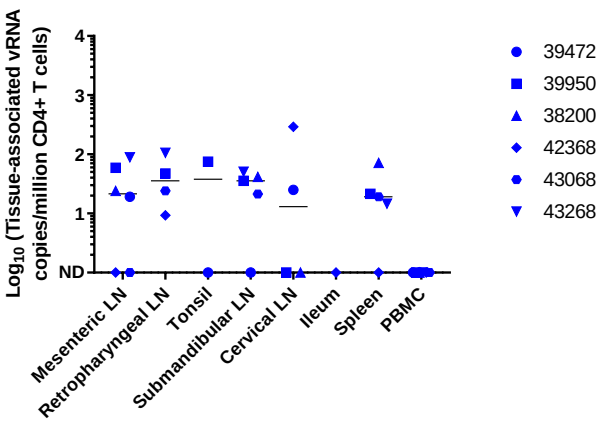

D.

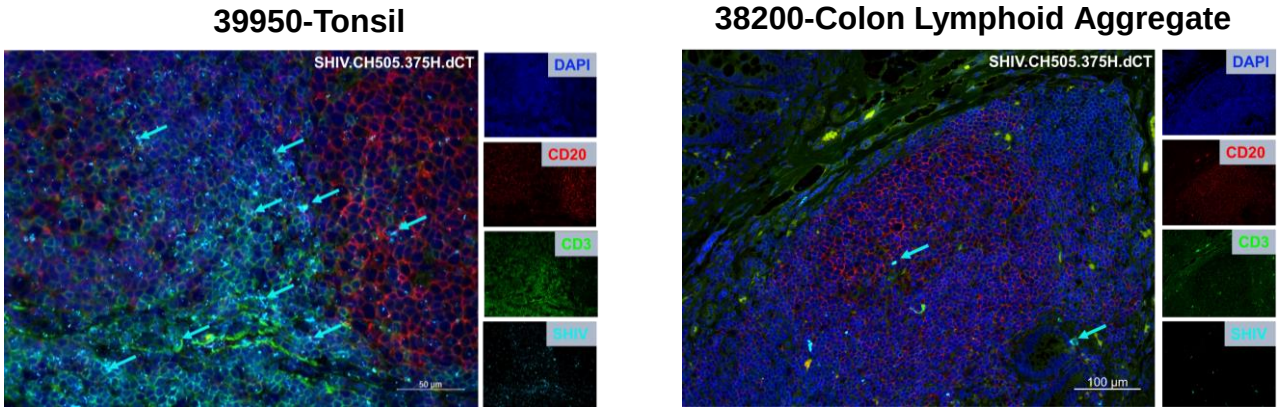

Figure 4: Tissue-associated infectious virus load upon ATI, in mononuclear cells isolated from PBMCs, lymphoid and GI tissues of adult RMs intravenously infected with SHIV.CH505.375H.dCT (A) Tissue-associated infectious SHIV.CH505.375H.dCT titers measured through tissue mononuclear cell coculture with Tzm-bl reporter cells. Reported titers represents the estimated minimum number of mononuclear cells per 10^4 mononuclear cells required to yield detectable infection of 50% Tzm-bl cells (CID_{50}). **(B)** CD4+ T cell-associated proviral DNA and **(C)** Viral RNA loads reported as copy number/million CD4+ T cells in PBMCs,

lymphoid and GI tissue mononuclear cells. Each symbol represents one individual monkey at necropsy (week 32 pi). Medians are indicated as horizontal lines on the dot plots. **(D)** Tonsil and colon sections from the SHIV.CH505.375H.dCT infected adult RM (39950) that demonstrated highest peak plasma VL post-rebound (13000 vRNA copies/mL plasma). Tissue sections were stained with the nuclear marker DAPI (dark blue) to identify cells, and with antibodies specific for CD3 (green) and CD20 (red). Virally-infected cells were identified by *in-situ* hybridization (cyan). Each panel consists of a larger image with the overlay of all markers and 4 smaller side panels of the same field for each individual channel. Arrow colors correspond to the indicated marker. The large image has a scale bar in the lower right corner.

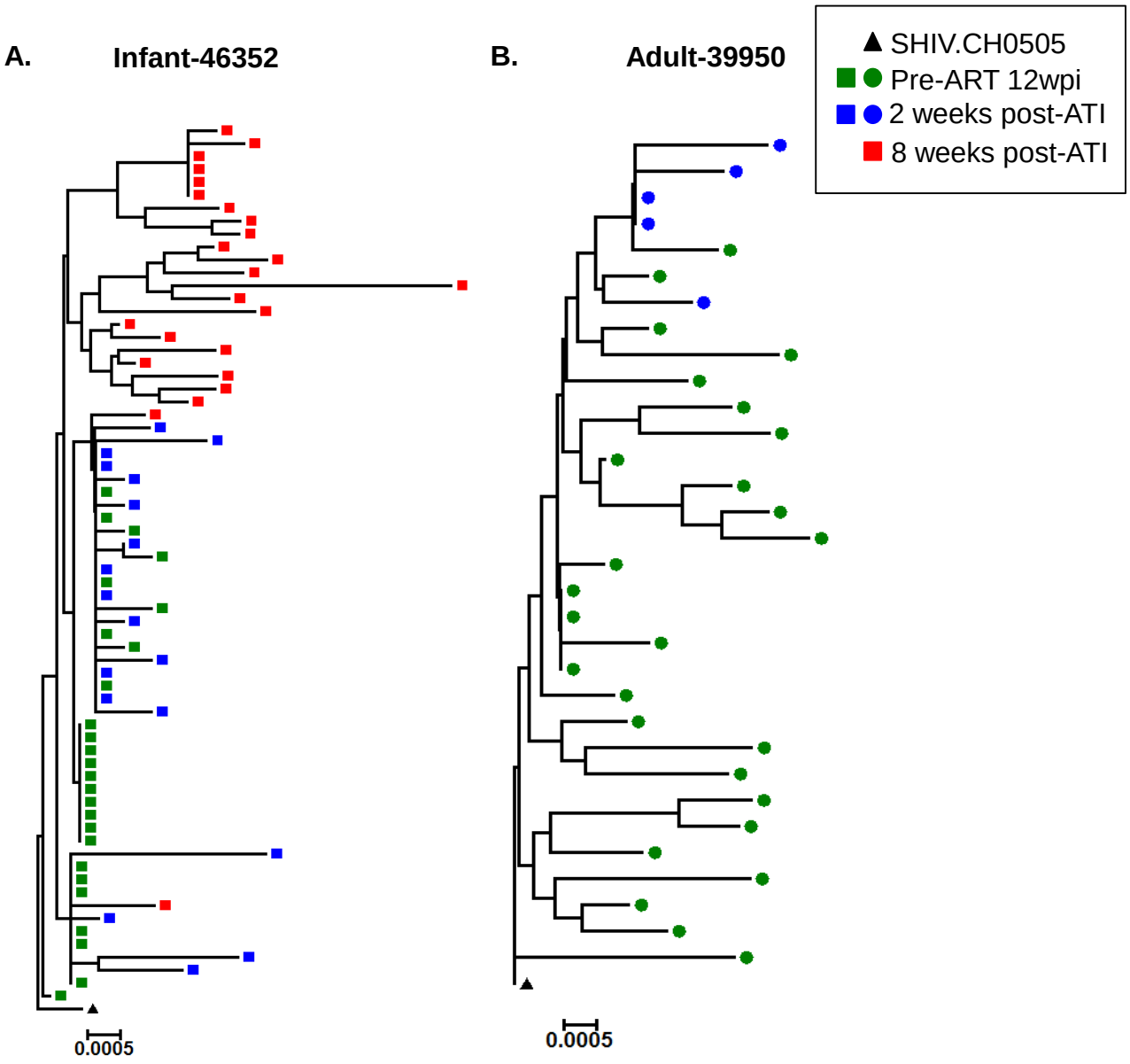

Figure 5. Phylogenetic tree analysis of the *env* gene sequences obtained from pre-ART and post-ATI plasma of infant and adult RM demonstrating highest peak plasma VL post-rebound. Standard SGA techniques were used to analyze the *env* gene from pre-ART and post-ATI samples of infants and adult RMs with highest peak rebound plasma VL. Phylogenetic tree representing viral Env diversity in **(A)** infant 46352 and **(B)** adult 39950.

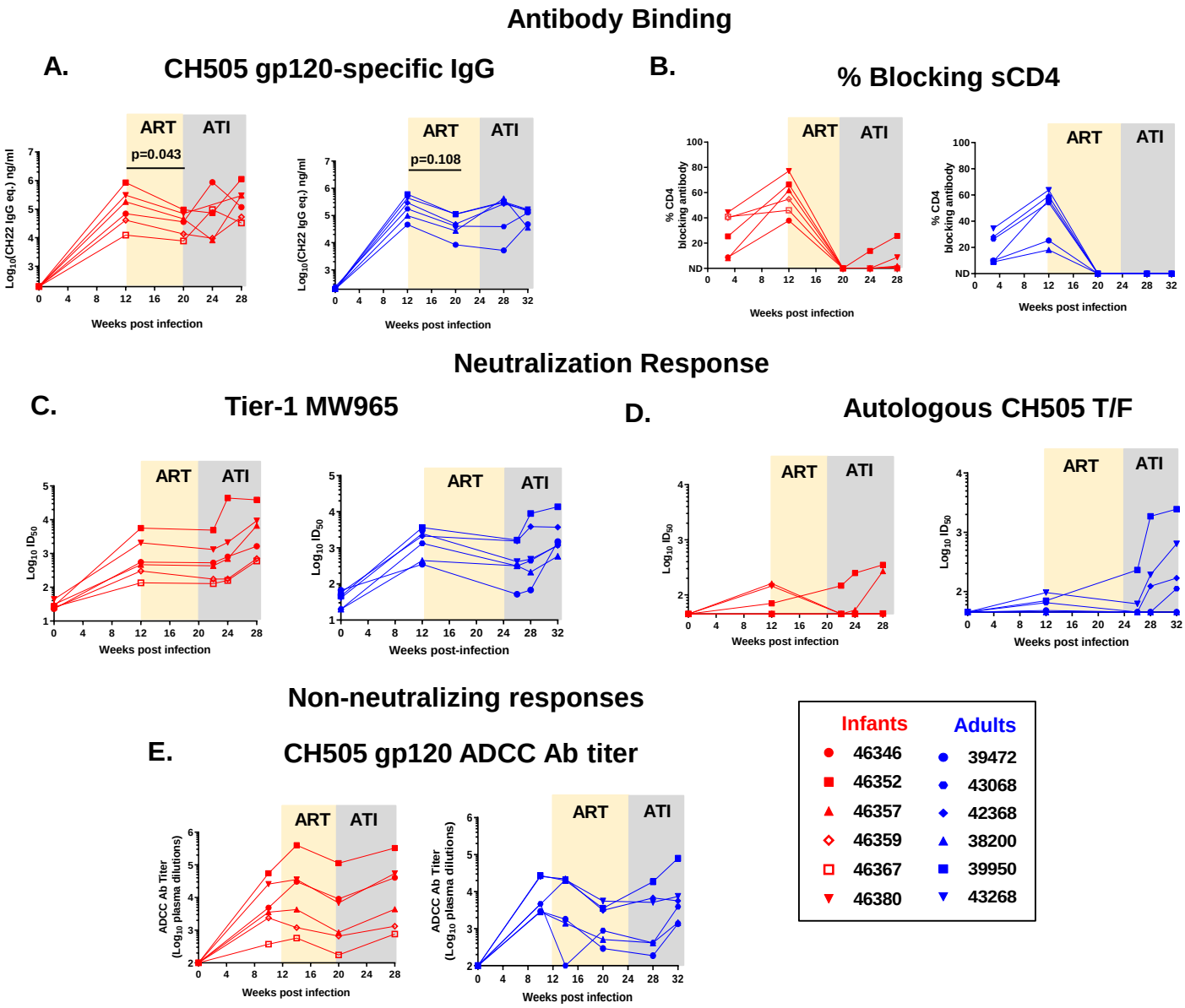

Figure 6: Magnitude and kinetics of humoral responses to acute SHIV.CH505.375H.dCT infection, during ART and ATI in RMs. Plasma from infant and adult rhesus macaques were analyzed for **(A)** HIV CH505 gp120 IgG response **(B)** blocking of soluble CD4-gp120 interactions **(C)** tier-1 neutralization response against MW965 **(D)** neutralization response against CH505 T/F, and **(E)** ADCC titer against CH505 gp120-coated target cells. Red symbols represent infant RMs and blue symbols represent adult RMs. Each symbol represents an individual macaque. Yellow and grey boxes represent duration of ART and duration of ATI in the RMs, respectively. Infants with plasma VL<15 copies/mL at 12 w.p.i has been represented with open symbols. P values were calculated using Wilcoxon signed rank test.

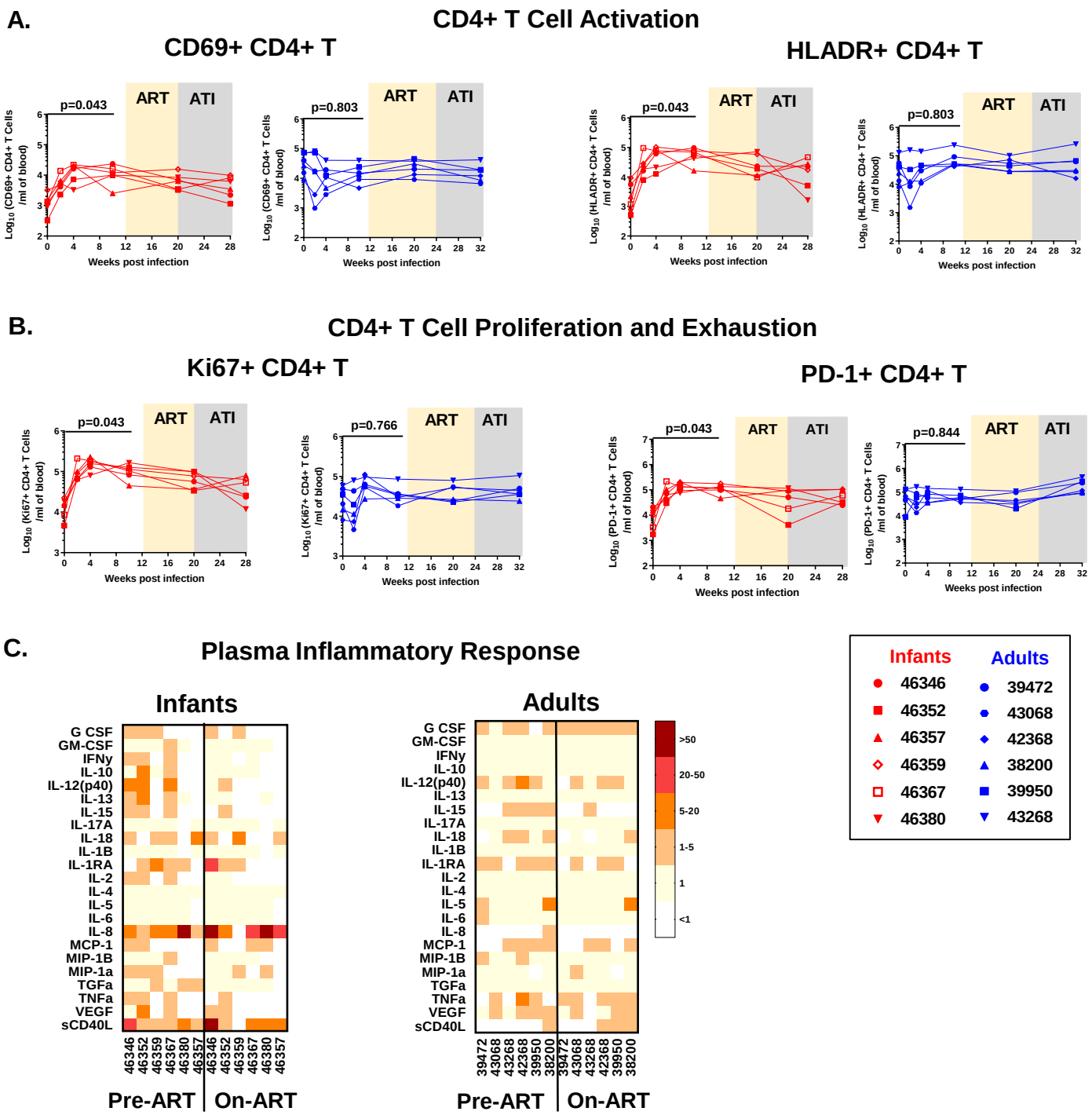

Figure 7: CD4+ T cell activation and plasma inflammatory responses in SHIV.CH505.375H.dCT infected infant and adult RMs. Absolute counts per ml blood of **(A)** activated (CD69+, HLADR+) CD4+ T cells and **(B)** proliferating (Ki67+ CD4+) and exhausted (PD-1+) CD4+ T cells. Red symbol represents infant RMs and blue symbols represents adult RMs. Each symbol represents one animal. Yellow and grey boxes represent duration of ART and duration of ATI, respectively. **(C)** Plasma from infected infant and adult RMs

were analyzed by multiplexed luminex assay for expression of cytokines before ART (week 12) and 8 weeks on ART (week 20). Heat map represents fold change of each analyte over pre-infection plasma levels. Infants with plasma VL<15 copies/mL at 12 w.p.i has been represented with open symbols. P values were calculated using Wilcoxon signed rank test.